NATIONAL ADVISORY COMMITTEE FOR AERONAUTICS

TECHNICAL NOTE 3040

USE OF TWO-DIMENSIONAL DATA IN ESTIMATING LOADS ON A 45° SWEPTBACK WING WITH SLATS AND PARTIAL-SPAN FLAPS

By Lynn W. Hunton and Harry A. James

Ames Aeronautical Laboratory
Moffett Field, Calif.

Washington
November 1953

1Q

NATIONAL ADVISORY COMMITTEE FOR AERONA

TECHNICAL NOTE 3040

USE OF TWO-DIMENSIONAL DATA IN ESTIMATING LOADS ON A 45° SWEPTBACK WING WITH SLATS AND PARTIAL-SPAN FLAPS

By Lynn W. Hunton and Harry A. James

SUMMARY

A study has been made of the application of two-dimensional data and span-loading theory for estimating the local loading characteristics on a swept wing with flaps. Estimated results, including local pressure distributions, span loadings, and the nonlinear local lift characteristics, are compared with similar results measured at large scale on a 45° sweptback wing of aspect ratio 6 having a 0.4-span double-slotted flap both with and without a full-span slat.

Two-dimensional pressure distributions when corrected for sweep were found to agree closely with the wing pressures for most local sections either on or off the flap. This agreement continued to the higher lift coefficients and even improved near maximum lift where the flap-induced effects became minimized. The Weissinger 7X1 method was found to provide reasonably accurate span loadings for this swept-wing configuration which had a relatively highly loaded type of flap. Two-dimensional lift data, together with span-loading theory, afforded quite accurate estimates of the local nonlinear lift characteristics, including maximum lift of sections outboard of the flap but were inadequate for inboard sections of the wing where the three-dimensional boundary-layer control exercises a dominant effect.

INTRODUCTION

Aerodynamic loads on wings with high-lift devices represent one of the critical loading conditions requiring attention in aircraft design. Since the number of plan forms which can be investigated experimentally is obviously limited, the importance of a reliable means of estimating such loads is apparent.

For unswept plan forms the procedures of references 1 and 2 have provided a means of estimating local section characteristics generally considered quite satisfactory for most engineering purposes. These procedures, which differ mainly in the manner of treatment of the loading at the flap discontinuity, involve one basic assumption, namely, that the influence of the three-dimensional character of the potential

flow associated with the finite wing is confined principally to the span-loading characteristics; and, hence, the local sections of the wing can, for the most part, be related to two-dimensional section characteristics. The practicality of this assumption was demonstrated originally in reference 3 for clean unswept tapered wings.

For the case of the swept wing, such an approach appeared to be a logical point at which to begin a study of means to estimate the local section characteristics. Accordingly, an analysis of the load distribution on two 45° sweptback wings of aspect ratio 6 was presented in reference 4 with the intent of evaluating to what extent the familiar straight-wing procedure had application to a swept wing. By slight revision of the method (i.e., account for the reduction due to sweep of the effective potential velocity), it was found in the unseparated lift range to give local loading characteristics in good agreement with experiment over most of the wing span, the exception being regions in close proximity to the root and tip.

The purpose of the present report is to extend the analysis of reference 4 to the case of a swept wing with slats and partial-span flaps. The success of any such load-estimating procedure depends, of course, on the accuracy of the span-loading theory in accounting not only for the effects of finite span, but also for the additional complicating factors of sweep and a partial-span high-lift device. For swept wings of moderate aspect ratio, the method of reference 5 has been found to give span loadings in good agreement with experiment and, hence, is the theory evaluated herein. Two-dimensional data required for the analysis were obtained in one of the Ames 7- by 10-foot wind tunnels. Pressure data on the large-scale swept wing were measured in the Ames 40- by 80-foot wind tunnel at a Mach number of 0.2 and Reynolds number of 8 million.

NOTATION

The data are presented in the form of standard NACA coefficients which are applicable to a full-span configuration. All pitching moments are referred to the quarter point of the mean aerodynamic chord.

C_L	lift coefficient, $\frac{\text{lift}}{qS}$
C_{L_α}	rate of change of wing lift coefficient with angle of attack, per deg
C_D	drag coefficient, $\frac{\text{drag}}{qS}$
C_m	pitching-moment coefficient, $\frac{\text{pitching moment}}{qS\bar{c}}$
G	spanwise loading coefficient, $\frac{c_l c}{2b}$

P	pressure coefficient, $\frac{p_l - p}{q}$
c_l	section lift coefficient, $\frac{\text{section lift}}{qc}$
c_{l_δ}	rate of change of section lift coefficient with flap deflection, per deg
c_{l_α}	rate of change of section lift coefficient with angle of attack, per deg
R	Reynolds number based on $\bar{c}$
S	area of semispan wing, sq ft
b	span of complete wing, ft
c	local chord measured parallel to plane of symmetry, ft
c'	local chord measured normal to reference sweep line, ft
$\bar{c}$	mean aerodynamic chord, $\frac{\int_0^{b/2} c^2 dy}{\int_0^{b/2} c\, dy}$, ft
c.p.	center of pressure, percent chord
p	free-stream static pressure, lb/sq ft
p_l	local static pressure, lb/sq ft
q	free-stream dynamic pressure, lb/sq ft
y	lateral coordinate
α	angle of attack of wing, deg
α_o	angle of attack of two-dimensional airfoils, deg
$\frac{d\alpha}{d\delta}$	flap lift-effectiveness parameter, $\frac{c_{l_\delta}}{c_{l_\alpha}}$
Δ	incremental value
δ	angle of deflection of flap, measured parallel to plane of symmetry, deg

η fraction of semispan

Λ sweep angle of the wing quarter-chord line, deg

Subscripts

f flap

H.L. hinge line

max maximum

Λ yawed flow

DESCRIPTION OF MODEL AND APPARATUS

Pertinent dimensions of the semispan wing-fuselage model are shown in figure 1. The basic wing is the same as used in the analysis of reference 4 and is referred to therein as the plain wing. The wing had 45° sweepback of the quarter-chord line, an aspect ratio of 6, a taper ratio of 0.5, and employed an NACA 64A010 section normal to the reference sweep line. A photograph of the test installation is shown in figure 2.

The partial-span flaps were of the double-slotted type and covered 0.4 semispan from 0.18 to 0.58 semispan, as defined by the midchord line of the flap in the retracted position. The leading-edge slat extended from the wing-fuselage juncture (0.14 semispan) to the wing tip. Details of the flap and slat configurations are shown in figure 3 by a typical section taken normal to the reference sweep line, and ordinates of each are given in table I. The wing was equipped with 7 pressure orifice stations, as shown in figure 1, with each station consisting of a minimum of 40 pressure orifices.

RESULTS AND DISCUSSION

This report deals with a simplified approach to the problem of determining the surface loadings on a swept wing having a partial-span high-lift flap wherein all three-dimensional effects are disregarded, with the exception of those accounted for in the span-loading theory. Accordingly, within the limitations of the data available, an attempt is made to demonstrate the extent to which load distributions, chordwise and spanwise, on the swept wing considered herein can be estimated using two-dimensional data corrected for sweep and the Weissinger span-loading theory. Studies of these two types of loadings, chordwise and spanwise, constitute two divisions of the report. A third section is directed

toward use of span-loading theory in conjunction with two-dimensional-lift data for estimating the local lift characteristics of sections, on and off the flap.

The longitudinal force characteristics for the two wing configurations considered herein are presented for reference purposes in figure 4, while in figure 5 are given the two-dimensional-lift characteristics for the four section configurations involved in the study. All wing data used throughout the report were obtained at a Mach number of 0.2 and Reynolds number of 8 million, based on the mean aerodynamic chord. The two-dimensional data were obtained at a Reynolds number of 4 million which corresponds closely with the average effective Reynolds number for the wing based on the components of mean aerodynamic chord and velocity, each taken normal to the wing quarter-chord line. The chordwise loading results involving correlations of pressure distribution and center of pressure are given in figures 6 to 9, while the spanwise loading and local lift-curve results are presented in figures 10 to 13.

Chordwise Loading

Method and results.- Because the method of correlation of section pressure data with the local loadings on the wing is basically the same as that described in reference 4, it is only briefly discussed here. In order to exclude any deficiencies of the span-loading theory from this chord-loading phase of the study, the estimated section pressure diagrams are based on measured values of local c_l rather than calculated values. Following sweep theory, the effective c_l on the swept wing which is to be related to unswept two-dimensional data is

$$c_{l_{\Lambda=0}} = \frac{c_{l_\Lambda}}{\cos^2\Lambda}$$

The two-dimensional pressure coefficients corresponding to these unswept values of $c_{l_{\Lambda=0}}$, in order to be compared to the swept wing, then, must be converted back to yawed flow conditions, thus

$$P_\Lambda = P_{\Lambda=0} \times \cos^2\Lambda$$

Pressure diagrams determined in this manner correspond to those which would be measured on the infinite airfoil in yawed flow.

Comparisons of estimated pressure distributions with those measured on the wing at six spanwise stations are shown in figures 6 and 7 for the flapped wing with slats retracted and extended. For both configurations

the correlations have been made for two angles of attack, one near 0° where separation is minimized and the other near $C_{l_{max}}$ to illustrate a typical design condition. The two indicated configurations of the wing involve four different configurations of the basic wing section, these being the NACA 64A010 clean, with slats, with double-slotted flaps, and with slats and flaps.

Loading at low α.- Correlations of loadings at six spanwise stations in figure 6 are given for angles of attack of the wing of 0° with slats retracted and 4.2° with slats extended. These angles represent for each configuration the lowest attitude of the wing for which correlations were possible with the available two-dimensional data. As mentioned earlier, the estimated pressure diagrams shown correspond to those for the appropriate profile in yawed flow with no adjustments being made for chordwise three-dimensional induction effects. Consequently, at the root station (0.17 semispan) where the orifice station lies between the inboard end of the flap and the fuselage, it is evident from the lack of correlation that the magnitude of the chordwise-induced loads renders any loading estimate, based on two-dimensional data, valueless in this region. Had the wing flap extended clear to the fuselage, then possibly a more satisfactory correlation would have resulted since not only would the flap extremity have been eliminated but the magnitude of plan-form-root effects very likely would have been dominated to a large extent by the flap-load increment.

For the two stations on the flap (0.38 and 0.55 semispan), the pressure distributions measured two-dimensionally and corrected to yawed flow show quite close agreement with experiment for either configuration of the flapped wing, slats retracted or extended (figs. 6(b) and 6(c)). The largest discrepancy can be seen to occur on the main flap at the inner station. The estimated flap loadings, even at this low angle of attack, seem to indicate the presence of some flow separation by the appearance of the pressure-recovery characteristics. Hence, the difference in loading noted at the inner station could arise from improved flow conditions on the wing flap, as a result of a boundary-layer-control action attendant with spanwise flow of the boundary-layer air. At the outer station on the flap where the boundary-layer action is weakened, the correlation can be seen to be much closer. The difference in loading at the inner station appears in figure 9 as an 8-percent rearward shift of local center of pressure.

Outboard of the flap, load comparisons are shown for three stations at 0.71, 0.82, and 0.92 semispan. Estimated results for these unflapped sections were derived from the pressure distributions of reference 6 for the NACA 64A010 section and from unpublished experimental data for this section with the slat extended. The largest discrepancy between the estimated and measured loadings is evident at the 0.71-semispan station where a portion of the loading induced by the flap is of the distributed camber type amounting to a shift aft in center of pressure of about 8-percent

chord. At stations further outboard, this effect virtually disappears, leaving very close agreement between the estimated and measured results.

Loading near maximum lift.– To demonstrate the applicability of the procedure for a critical design condition near stall, pressure-distribution comparisons are given in figure 7 for an α of 8.4° and C_L of 1.07 for the wing with slats retracted and for an α of 12.4° and C_L of 1.31 with the slats extended. It will be noted for these high-lift comparisons that all values of local c_l on the wing for either configuration have exceeded the appropriate two-dimensional $c_{l_{max}}$ values when corrected to yawed flow. Such a condition is normal for swept wings where it has been reasoned that an effective boundary-layer-control action exists over the entire span, being a maximum near the root and diminishing spanwise to virtually no effect at the wing tip (described in analysis of ref. 4). Recognition of these conditions obviously poses two problems in the prediction of maximum loads for a swept wing; first, of how to estimate the $c_{l_{max}}$ potential of various sections of the wing initially, and, second, knowing the $c_{l_{max}}$ values, how to estimate the chordwise loading with available two-dimensional data limited in the c_l range as it is. The former problem will be discussed in another section of the report while the latter is of immediate concern here. The limited range of the two-dimensional data indicates that some means of extrapolation to higher values of lift is necessary if correlations are to be made near maximum lift. For the comparisons herein, different procedures were followed for the two wing configurations considered. With slats retracted the two-dimensional pressure distributions for unflapped sections are from airfoil theory of reference 7, while those for the flapped sections are simply the basic pressure distribution measured two-dimensionally at an angle of attack of 0° with the addition of theoretical pressures due to additional type lift for the NACA 64A010 section of sufficient amount to obtain the desired c_l. With slats extended the use of theoretical pressure distributions becomes difficult to apply. Therefore, an alternative procedure was employed whereby the two-dimensional pressure distributions for the required c_l values were reached by linear extrapolations of the two-dimensional pressure data. This procedure has been followed for slatted sections of the wing, both on and off the flap.

Inspection of these results near $C_{L_{max}}$ for an over-all comparison with the previous results at lower C_L reveals that only small differences exist, and these, in general, are in the direction of improvements in the correlation. At the root station inboard of the flap, the loading on the wing continues to be dominated by three-dimensional chordwise loading effects; hence, this region obviously is beyond the applicable range of this simplified method. Both stations on the flap with or without slats show generally close correlation between the estimated and measured results, thus signifying little flow separation at this high C_L. For the three stations outboard of the flap, virtually all evidence of the induced camber effect has disappeared at these higher lifts as a result of the dominance of additional type lift. It is clear, therefore, that the use of two-dimensional data or theory together with sweep theory

provided a reasonably accurate indication of local loads over the major part of this wing for lift coefficients approaching those for stall. However, in view of the simplifying assumptions involved, it is anticipated some difficulty would be encountered in estimating the loads close to the root, tip, or flap junctures. The results herein demonstrated such a difficulty only in the case of the root section load but were not sufficiently detailed to cover loadings beyond 92-percent semispan nor closer to the flap junctures than 5-percent semispan.

Use of streamwise section data.- Figure 8 is presented for the purpose of briefly illustrating the importance of accounting for the effects of sweep when estimating the local loadings over the flapped portions of swept wings. The data shown for the wing were measured at the 0.55-semispan station with the orifices oriented in a streamwise direction. Data for angles of attack of the wing of 0° and 8° are shown for configurations of the slat retracted and extended, respectively. Section data for these comparisons were obtained from two-dimensional tests of two sections approximating the two streamwise section configurations of the wing. For these tests the same basic models as used for the preceding analysis were tested with the flap, vane, and slat deflection angles adjusted to values appropriate for the profile of the wing parallel to the free stream. Obviously, this is an approximation where the principal deviation involves the section maximum thickness. However, the main effect of this difference would be to shift the level of the pressures a small amount without materially altering the magnitude or distribution of either the basic flap load or the induced load on the main section. These data are compared directly (uncorrected for sweep) with the wing data for equal values of c_l. The results clearly demonstrate a complete lack of any correlation by this method. The two-dimensional data can be seen to indicate loads over the flap and vane almost double those for the wing. Consequently, to attain the wing c_l values, the two-dimensional pressures must be obtained at very low angles of attack with attendant negative loads on the slat or leading edge of the section. It is recognized the only available streamwise station on the flap falls rather close to the flap extremity (fig. 1) where, it might be argued, end effects would confuse the correlation. That this is not the case (or at least an insignificant effect compared with the discrepancies noted in these streamwise-loading correlations) is borne out by the close comparison of this streamwise section flap loading on the wing in figure 8 with the comparable chordwise section flap loading in figure 6(c), both for an α of 0° and the slats retracted configuration.

Spanwise Loading

Method and results.- The theoretical loadings were calculated by the Weissinger 7X1 method of reference 5. In this method loadings for arbitrary flap spans involve an interpolation procedure which, for the flap configuration of this report, is illustrated in figure 11. In

part (a) are shown the loadings for the four flap spans for which direct solutions are available, while in part (b) cross-plotted results are given of the variation of the loading parameter at given stations (0.1-semispan increments) as a function of flap span. A $d\alpha/d\delta$ value of 0.5 was used which was derived from the available two-dimensional data. Slat configuration did not affect this value. The calculated flap loadings of figure 10 are based on a 0.4-span flap extending from 0.18 to 0.58 semispan and on a streamwise section flap deflection angle of 47° based on the hinge-line sweep angle following the relation

$$\tan \delta_{stream} = \tan \delta_{normal} \times \cos \Lambda_{H.L.}$$

The theoretical loadings near $C_{l_{max}}$ were determined for the same values of wing C_L as measured experimentally and consist of the fixed-flap incremental loading plus the necessary amount of additional type loading to make up the total C_L required. The experimental loadings undoubtedly contain a fuselage-interference effect but, in view of an uncertainty as to the influence of the tunnel-floor boundary layer on the fuselage loading, consideration of the effect has been disregarded throughout these calculated results.

Comparisons of experimental and theoretical span loadings for both configurations of the wing are given in figure 10 for 0° angle of attack and for an angle of attack near $C_{l_{max}}$. Experimental points are indicated for the same six pressure stations used in the pressure-distribution study. The spanwise locations of five of the stations oriented in a chordwise direction have been chosen as the intersection of the station with the quarter-chord line, inasmuch as additional type lift is centered near this point. Obviously, for low angles of attack the point selected represents rather a rough approximation, especially for sections involving the flap, but in approaching $C_{l_{max}}$ the assumption becomes more justifiable.

Loading at $\alpha = 0°$ (flap lift increment).- Owing to the effect of a slat on the angle for zero lift, the loadings at an α of 0° for the two wing configurations differ by a small amount. Thus, in figure 10, only the loading with slats retracted strictly indicates the flap lift increment; integration of the calculated loading (weighted by local chords) for this case gives a ΔC_L of 0.62 which compares favorably with a measured value for the wing of 0.59. With slats extended the theoretical loading shown has been reduced by an incremental additional type loading amounting to 0.04 in C_L as an approximation of the full-span-slat effect. The value of 0.04 was derived from the two-dimensional-slat results corrected for sweep. The resultant C_L values for these zero-angle loadings are 0.58 for the calculated compared with 0.57 measured.

The calculated distributions of loading based on interpolated results at 0.1-semispan increments appear to be in reasonably good agreement with the experimental points. The most noticeable deficiency of the

theory is a failure to account fully for the difference in loading between flapped and unflapped sections of the wing. This discrepancy most likely stems from a limitation of the theory, mentioned in reference 5, in accurately accounting for discontinuous twist distributions, especially of the magnitude introduced by the relatively efficient double-slotted flap.

Loading near $C_{L_{max}}$.- The span-load distributions in figure 10 include comparisons for lift coefficients of 1.07 and 1.31, slats retracted and extended, respectively, which closely approach the measured $C_{L_{max}}$ values of 1.17 and 1.47. It is significant to note that at these high lifts the accuracy of the theory shows no sign of deteriorating from that noted for the lower lift case. In fact, with slats extended, the correlations even show some improvement at this higher lift. The obvious reason for this success is the absence of any significant amount of flow separation. Similar accuracy of the method is obtainable for this wing without flaps, as noted in reference 4, although in this case the C_L range for accuracy did not extend as close to $C_{L_{max}}$ owing to the more gradual progression inboard of flow separation.

Local Lift Curves

While potential-flow calculations yield generally reliable span-loading results, such theories in not accounting for viscosity, of course, cannot provide for a given wing any clue to separation or maximum lift. For straight wings this important boundary-layer information has been supplied quite successfully through two-dimensional experimental results, as demonstrated in reference 2. With inclusion of sweep, however, the boundary-layer characteristics are altered somewhat as a consequence of the greatly increased amount of lateral flow of the boundary layer. By comparison, then, of two-dimensional lift data with the measured results on the swept wing, it would be expected some knowledge could be gained regarding the nature and magnitude of the viscous effects which ultimately should be useful in estimating the stall behavior of a wing approximating the general configuration considered.

Method and results.- Local lift data for both wing configurations are given in figure 12. For each of the six stations of the wing there is also given an estimated lift curve, based on the two-dimensional results of figure 5 and span-loading theory. The estimation procedure basically follows that described in reference 4 wherein three steps are indicated: (a) conversion of the two-dimensional lift curves to yawed flow conditions, (b) adjustment of the lift-curve slopes to account for local induced angle-of-attack characteristics on the finite wing, and (c) orientation of the estimated local lift curves to the wing angle of attack.

For the first step, following the theory of sweep, the angles of attack and corresponding values of lift coefficient for the equivalent yawed infinite wing become:

$$\alpha_{o_\Lambda} = \alpha_{o_{\Lambda=o}} \times \cos \Lambda$$

$$c_{l_\Lambda} = c_{l_{\Lambda=o}} \times \cos^2 \Lambda$$

Next, to account for the local induced angles of attack on the finite wing and, hence, spanwise variation in lift-curve slope, the foregoing yawed infinite wing lift curves were then modified so that the slopes in the linear or near linear lift range matched those given by the Weissinger theory.[1] This step was accomplished by adjusting only the angle-of-attack values and leaving all corresponding values of lift coefficient the same as those for the yawed infinite wing, thus

$$\alpha_{local} = \alpha_{o_\Lambda} \times \frac{(c_{l_\alpha})_{\text{yawed infinite wing}}}{(c_{l_\alpha})_{\text{finite wing theory}}}$$

$$c_{l_{local}} = c_{l_\Lambda} = c_{l_{\Lambda=o}} \times \cos^2 \Lambda$$

Finally, for configurations involving other than zero loading at zero wing angle of attack, an additional step is required to orient these estimated local lift curves to the wing angle of attack. The loading for a given value of wing angle of attack (0° for this case) must be computed from theory. For the flapped sections of the wing the estimated lift curves were shifted by an increment in angle of attack so as to intercept the calculated values of local c_l at 0° angle of attack. For the unflapped sections a different procedure would seem advisable in view of experience with straight wings. For the straight wing it has been the practice to increase all two-dimensional values of c_l, including $c_{l_{max}}$, by some increment to account for increased maximum lifts of these sections found to exist apparently as a result of the camber-type load induced by the flap. In reference 2 a special correction factor is introduced for this purpose in estimating the local lift characteristics of unswept wings. Herein an alternative procedure is employed which is believed to be generally more straightforward in application, as well as more accurate for the swept-wing case. This procedure for the unflapped sections of the wing consists of increasing all values of c_{l_Λ} by the increment induced by the flap at 0° angle of attack given directly by the span-loading theory.

---

[1]Since only linear section lift curves are considered in the Weissinger span-loading theory, a simplifying assumption is made for purposes of the procedure of this report, wherein any induced effects associated with nonlinearities in section lift curves across the span of the wing are assumed to be small enough to be disregarded.

Low-lift characteristics.- At low angles of attack the degree of correlation shown in figure 12 between estimated and measured results with respect to either the level or slope of the curves obviously reflects directly the accuracy of the span-loading theory previously discussed. With slats retracted the theoretical slopes at several stations are slightly higher than experiment, giving an over-all C_{l_α} of 0.058 compared to a measured value of 0.056; whereas with slats extended the reverse trend is evident, with theory unchanged at a C_{l_α} of 0.058 compared with a measured over-all value of 0.059.

Maximum lift characteristics.- The estimated values of $c_{l_{max}}$ can be seen in figure 12 to fall somewhat short of experiment over the flapped sections of the wing, while for sections outboard of the flap reasonably close agreement is shown. To study these results in a little more detail in an attempt to isolate, if possible, some of the factors responsible for these differences in stall behavior between flapped and unflapped regions of the wing, figure 13 has been prepared. This figure shows the variation spanwise of the increment in $c_{l_{max}}$ measured over and above the two-dimensional value corrected for sweep. Included in the figure, along with the increments for the two wing configurations of this report, is a basic curve shown solid which represents the clean wing with no high-lift devices (from ref. 4). In the analysis of this reference, it was concluded that the variation spanwise in local $c_{l_{max}}$ found for the clean wing was indicative of the strength of the natural boundary-layer control associated with sweptback wings, the effect being a maximum at the root and diminishing gradually spanwise to little effect at the tip. In figure 13 it can be seen that the increments in $c_{l_{max}}$ for both stations on the flap of either wing configuration match closely the clean-wing increment. This would seem to suggest that the magnitude of the effective boundary-layer control in this region of the wing is governed primarily by the plan-form geometry since it is not materially altered, even by such severe changes in section and effective twist as introduced by a deflected flap. This inference is further substantiated by results of tests of this same plan form incorporating relatively large amounts of camber and twist (NACA 64A810 section with 10° washout) for which virtually identical increments in $c_{l_{max}}$ were found (see ref. 4).

In the case of sections outboard of the flap, the increments in maximum lift above the yawed infinite-wing values can be seen to rise above the clean-wing curve, the largest difference occurring close to the flap juncture. This result, it seems, illustrates the relative magnitudes of the two principal factors contributing to the $c_{l_{max}}$ increments in this region, namely, the natural boundary-layer-control effect indicated by the clean-wing curve with the remainder of the increment being chargeable to camber loading induced by the flap.

Returning to the estimated lift characteristics of figure 12, some explanation is seen for the difference in accuracy of the estimates of $c_{l_{max}}$ for the flapped and unflapped regions of the wing. For the flapped sections the estimated curves, as described previously, were derived from two-dimensional results and, hence, fall short of experiment

evidently by an amount governed by the strength of the spanwise boundary-layer flow. Owing to this effect, further progress in the estimation of the maximum lift characteristics of swept wings appears at an impasse until such time as some reliable means is found for predicting for any given wing increments in lift such as those illustrated in figure 13. In the case of the unflapped section $c_{l_{max}}$ estimates indicated in figure 12, all infinite wing values were increased by the amount of lift induced by the flap at 0° angle of attack of the wing, as given by span-loading theory; justification for this procedure is based on a reasoning that the flap-induced loads can be considered analogous to camber-type load and, hence, roughly additive to the potential $c_{l_{max}}$ of the section. While the results of both the pressure-distribution study of a previous section of the report and the incremental $c_{l_{max}}$ considerations in this section do not entirely substantiate the validity of the assumption, the method nevertheless provides for this wing a fairly accurate indication of the combined effects from the induced potential field and the three-dimensional boundary-layer control for sections outboard of the flap.

CONCLUSIONS

A study to determine the applicability of two-dimensional data for estimating loads on a sweptback wing with slats and partial-span flaps has been made and the following conclusions reached:

1. Correlations of wing pressure data with two-dimensional pressure data corrected to yawed flow conditions for profiles matching the section of the wing normal to the quarter-chord line indicated that:

   (a) For stations intersecting the flap, very close agreement with experiment was obtained for each component of the flapped section, this condition extending to lift coefficients just below stall.

   (b) For stations outboard of the flap, use of simple additional type loading gave good agreement with experiment, especially at lift coefficients approaching stall. At lower lift coefficients there was evidence of an induced camber-type loading from the flap which was restricted principally to the area adjoining the flap discontinuity.

   (c) Extension of a full-span slat produced no significant change in the foregoing conclusions.

2. Correlations of two-dimensional pressure data uncorrected for sweep with measured wing data, each for a section in a streamwise direction across the flap, revealed no agreement whatsoever.

3. A span-loading theory (simplified lifting surface) is demonstrated to provide for this wing an accurate estimate of the magnitude of the flap incremental loading at $\alpha = 0^\circ$, based on two-dimensional

values of $d\alpha/d\delta$, as well as a good indication of the distribution of spanwise loading.

4. Quite accurate estimates of $c_{l_{max}}$ were obtained for sections outboard of the flap, based on two-dimensional values of $c_{l_{max}}$ corrected for sweep and adjusted for the induced c_l increment from the flap.

5. A correlation of the measured $c_{l_{max}}$ values across the span of the flapped wing, with and without slats, with those for the wing in a clean condition revealed marked similarities in stall pattern. The results appeared to indicate that the influence of the spanwise flow of boundary layer in alleviating separation with resultant increases in $c_{l_{max}}$ is not affected particularly by drastic changes in section.

Ames Aeronautical Laboratory
National Advisory Committee for Aeronautics
Moffett Field, Calif., Aug. 19, 1953

REFERENCES

1. Pearson, Henry A., and Anderson, Raymond, F.: Calculation of the Aerodynamic Characteristics of Tapered Wings with Partial-Span Flaps. NACA Rep. 665, 1939.

2. Sivells, James C., and Westrick, Gertrude C.: Method for Calculating Lift Distributions for Unswept Wings with Flaps or Ailerons by Use of Nonlinear Section Lift Data. NACA TN 2283, 1951.

3. Anderson, Raymond F.: Determination of the Characteristics of Tapered Wings. NACA Rep. 572, 1936.

4. Hunton, Lynn W.: Effects of Finite Span on the Section Characteristics of Two 45° Swept-Back Wings of Aspect Ratio 6. NACA TN 3008, 1953. (Formerly NACA RM A52A10).

5. DeYoung, John: Theoretical Symmetric Span Loading Due to Flap Deflection for Wings of Arbitrary Plan Form at Subsonic Speeds. NACA TN 2278, 1951.

6. Peterson, Robert F.: The Boundary-layer and Stalling Characteristics of the NACA 64A010 Airfoil Section. NACA TN 2235, 1950.

7. Loftin, Laurence K., Jr.: Theoretical and Experimental Data for a Number of NACA 6A-Series Airfoil Sections. NACA Rep. 903, 1948.

TABLE I.- COORDINATES OF THE SLAT AND DOUBLE-SLOTTED FLAP

[Stations and ordinates given in percent of airfoil chord]

(a) Slat

Station	Upper ordinate	Lower ordinate
0	Same as NACA 64A010	Same as NACA 64A010
↓	↓	↓
4.68		-2.26
5.00		-1.36
5.50		-.56
6.00		-.02
7.50		1.05
10.00		2.11
15.00		3.46
17.00		3.95
L.E. radius: 0.69		
T.E. radius: 0.02		

(b) Vane

Station	Upper ordinate	Lower ordinate
0	0	0
.42	.95	-.93
.83	1.31	-1.14
1.25	1.52	-1.20
1.67	1.67	-1.11
2.08	1.72	-.85
2.92	1.74	-.36
3.75	1.64	-.02
4.58	1.43	.18
5.42	1.13	.27
6.25	.75	.25
7.08	.28	.11
7.50	0	0
L.E. radius: 1.20 (center on flap chord line)		

(c) Flap

Station	Upper ordinate	Upper ordinate
0	-1.00	-1.00
.15	-.37	-1.56
.30	-.08	-1.71
.59	.27	-1.96
.88	.54	-2.10
1.18	.75	-2.18
1.77	1.06	-2.29
2.35	1.27	-2.32
2.94	1.41	-2.30
3.53	1.50	-2.26
4.71	1.59	-2.14
5.88	1.64	-2.00
7.06	1.65	-1.88
8.24	1.63	-1.76
9.41	1.58	-1.64
10.00	1.55	-1.58
11.25	1.45	-1.45
15.00	1.06	-1.06
20.00	.54	-.54
25.00	.02	-.02
L.E. radius: 0.95 (center on flap chord line)		
T.E. radius: 0.02		

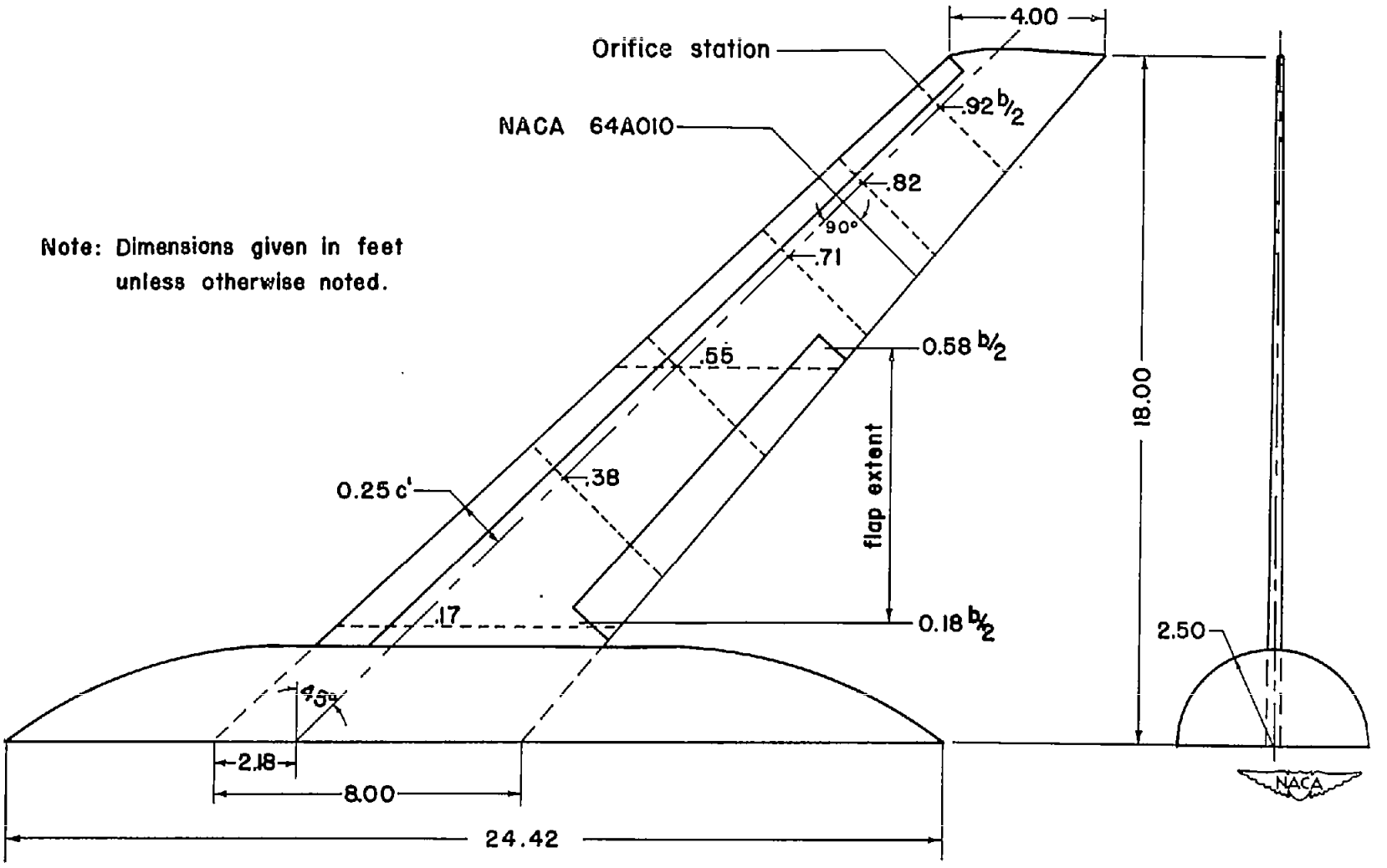

Figure 1.– Dimensions of the semispan wing–fuselage model including the orifice station locations.

Figure 2.- View of semispan wing-fuselage model installation in the Ames 40- by 80-foot wind tunnel.

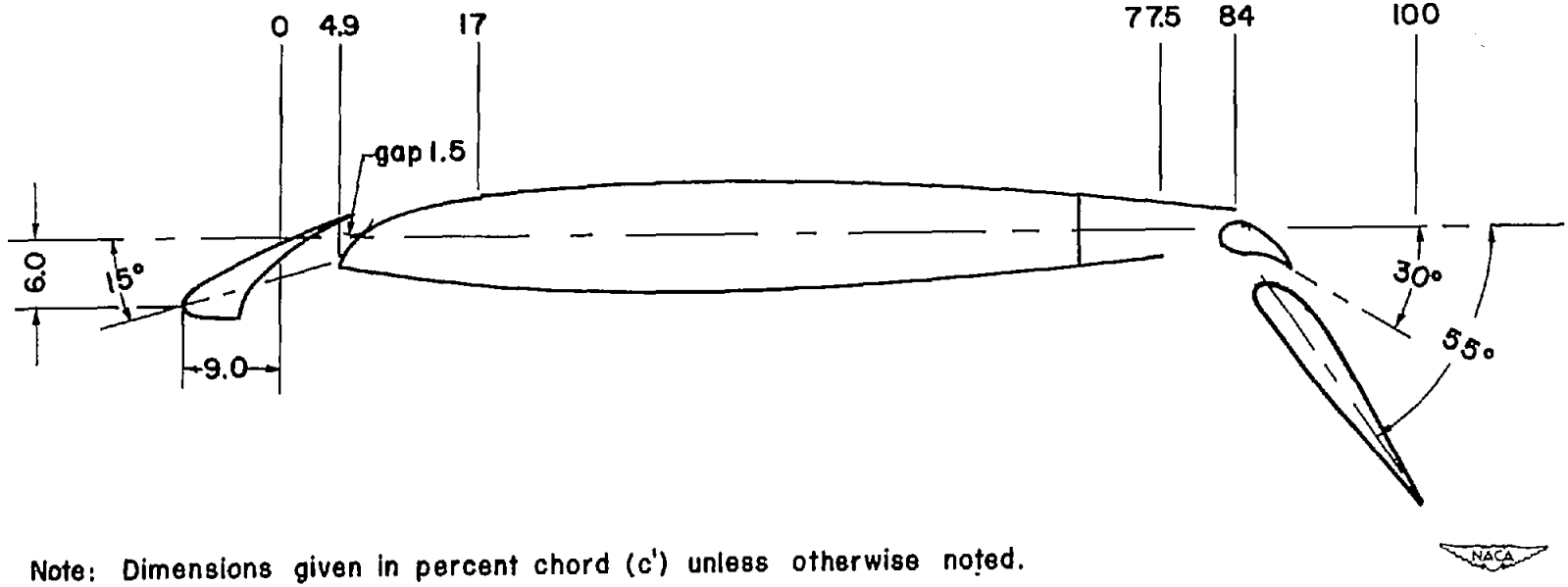

Note: Dimensions given in percent chord (c') unless otherwise noted.

Figure 3.– Details of the slat and double–slotted flap configuration for a section normal to the reference sweep line.

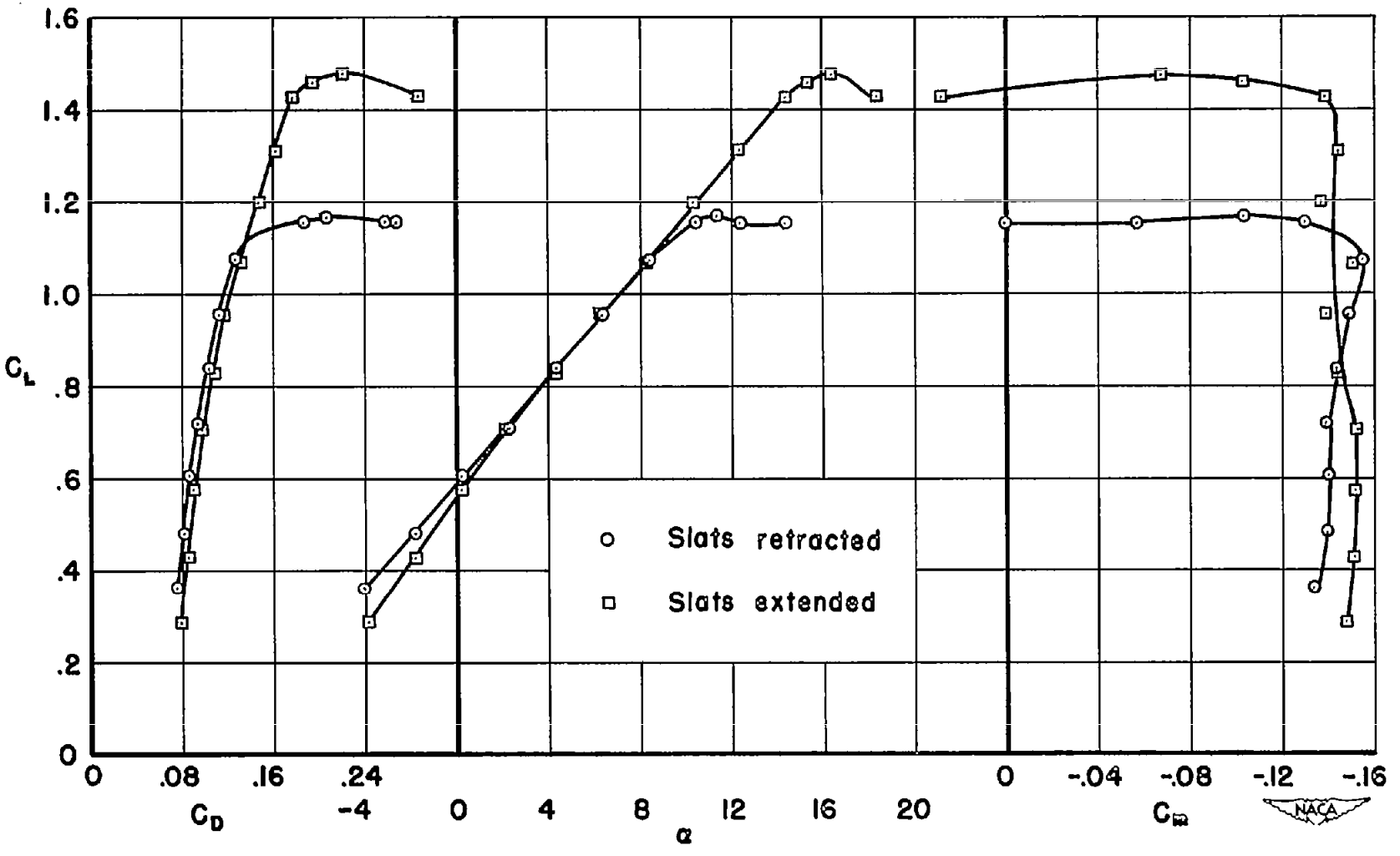

Figure 4.– Lift, drag, and pitching-moment characteristics of the model with flaps deflected, with and without slats extended.

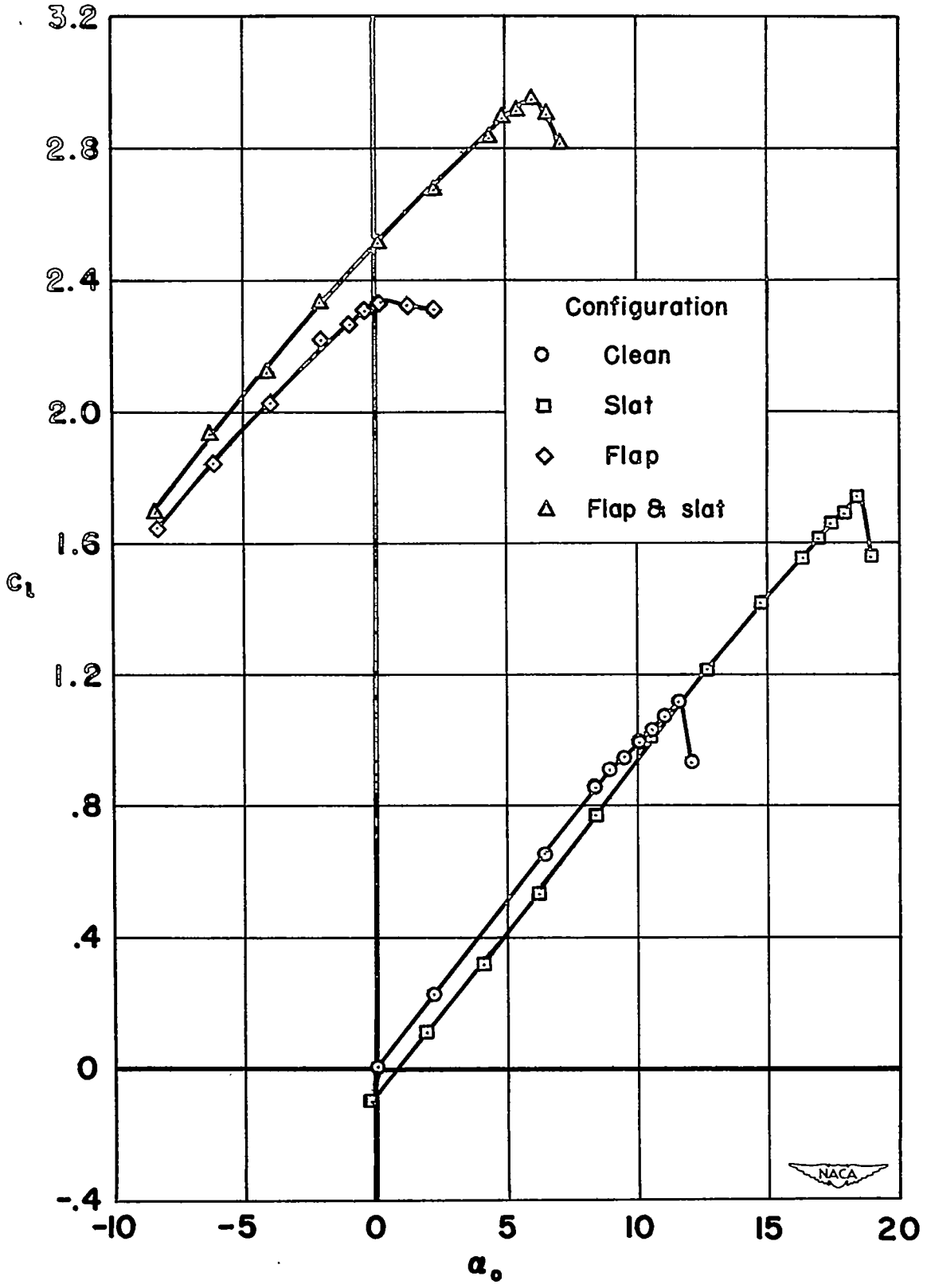

Figure 5.— Two-dimensional lift characteristics of the NACA 64A010 section with various combinations of slats and double-slotted flaps.

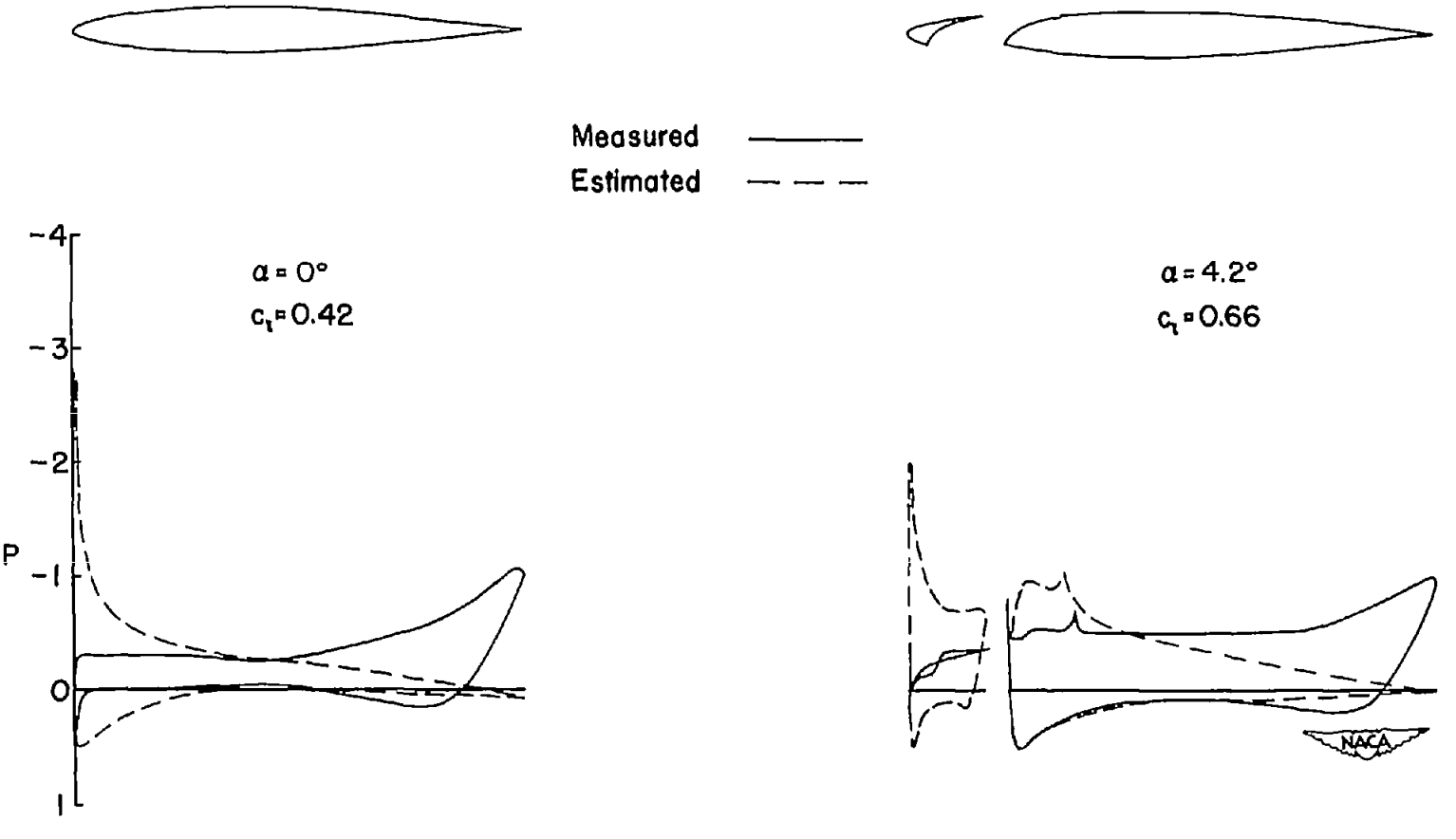

(a) $\eta = 0.17$

Figure 6.– Comparisons at low angle of attack of measured and estimated pressure distributions at six semispan stations with and without slats. Flaps deflected.

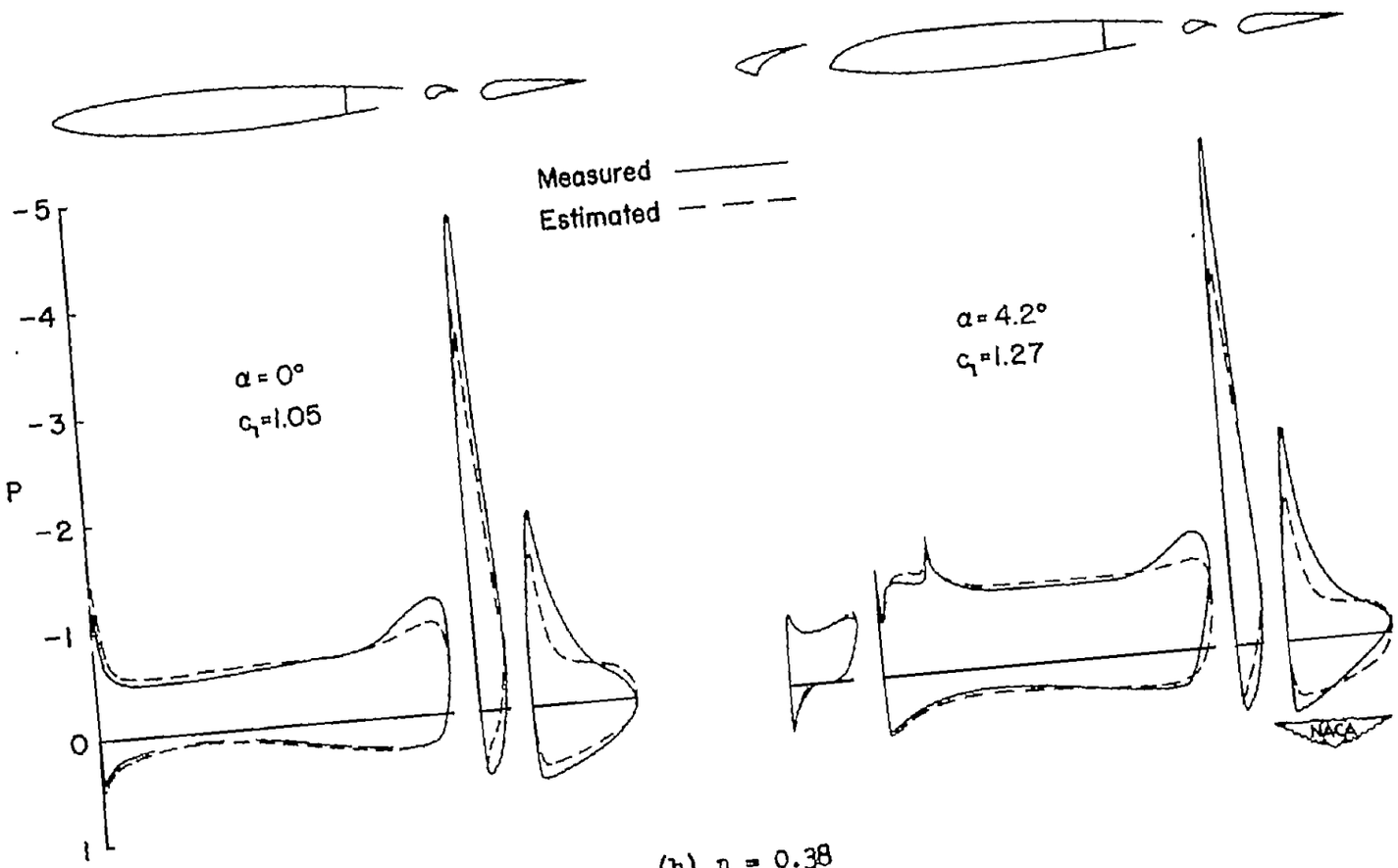

(b) η = 0.38

Figure 6.– Continued.

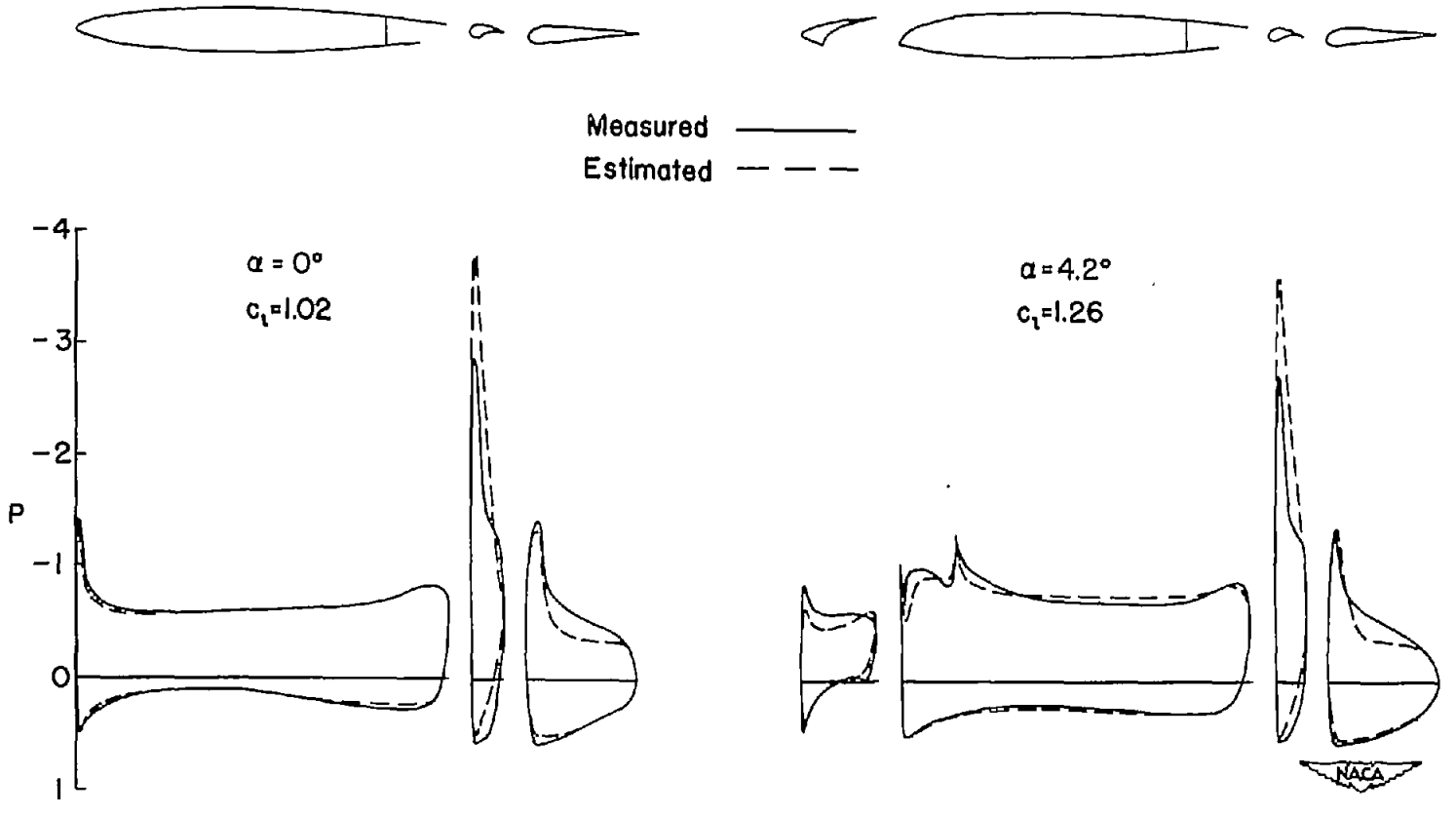

(a) η = 0.55

Figure 6.– Continued.

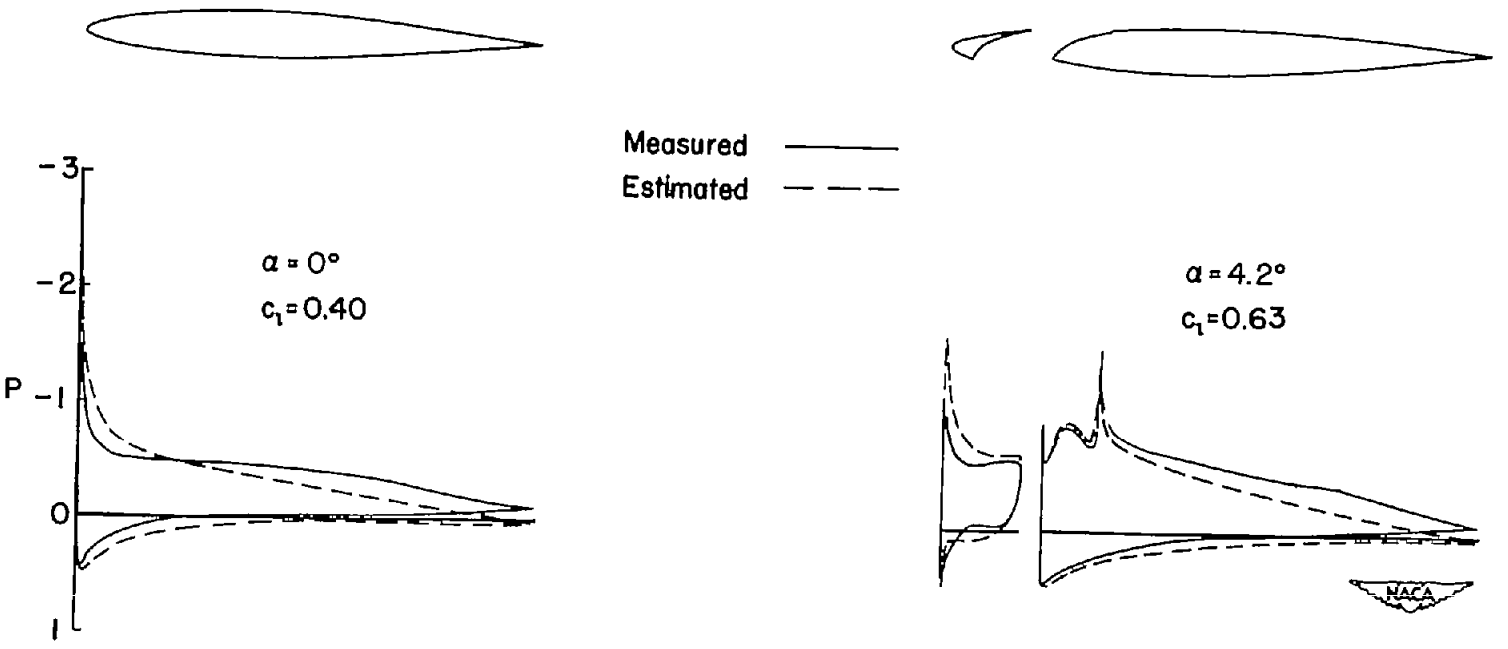

(d) η = 0.71

Figure 6.– Continued.

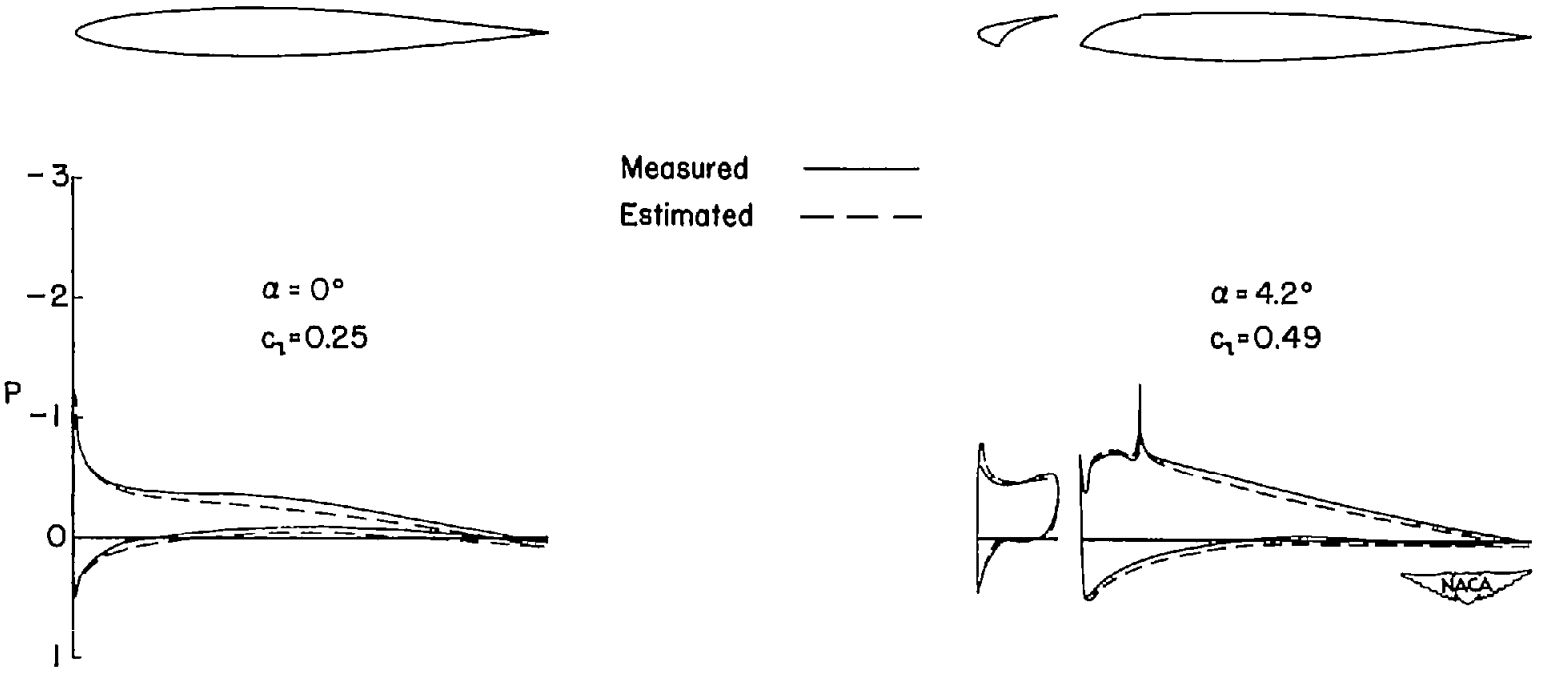

(e) η = 0.82

Figure 6.– Continued.

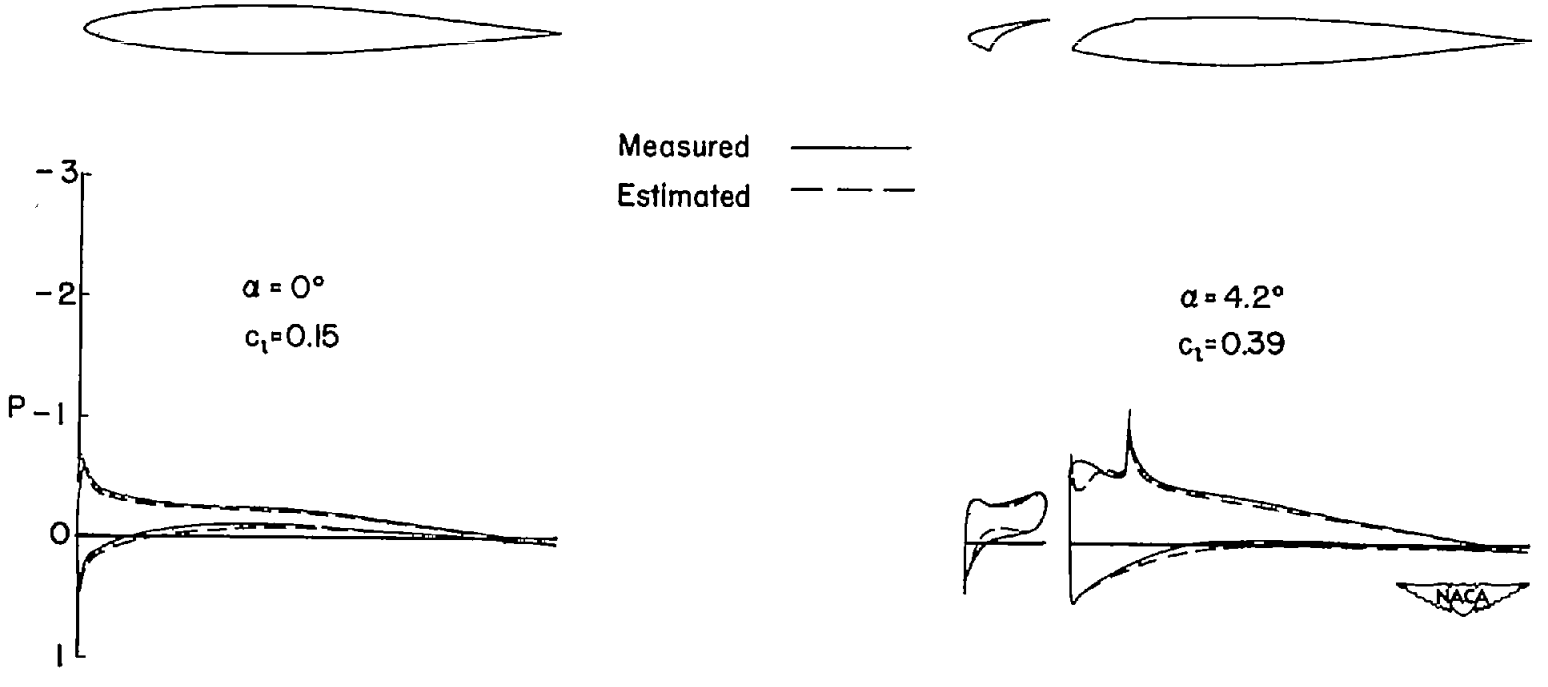

(f) η = 0.92

Figure 6.– Concluded.

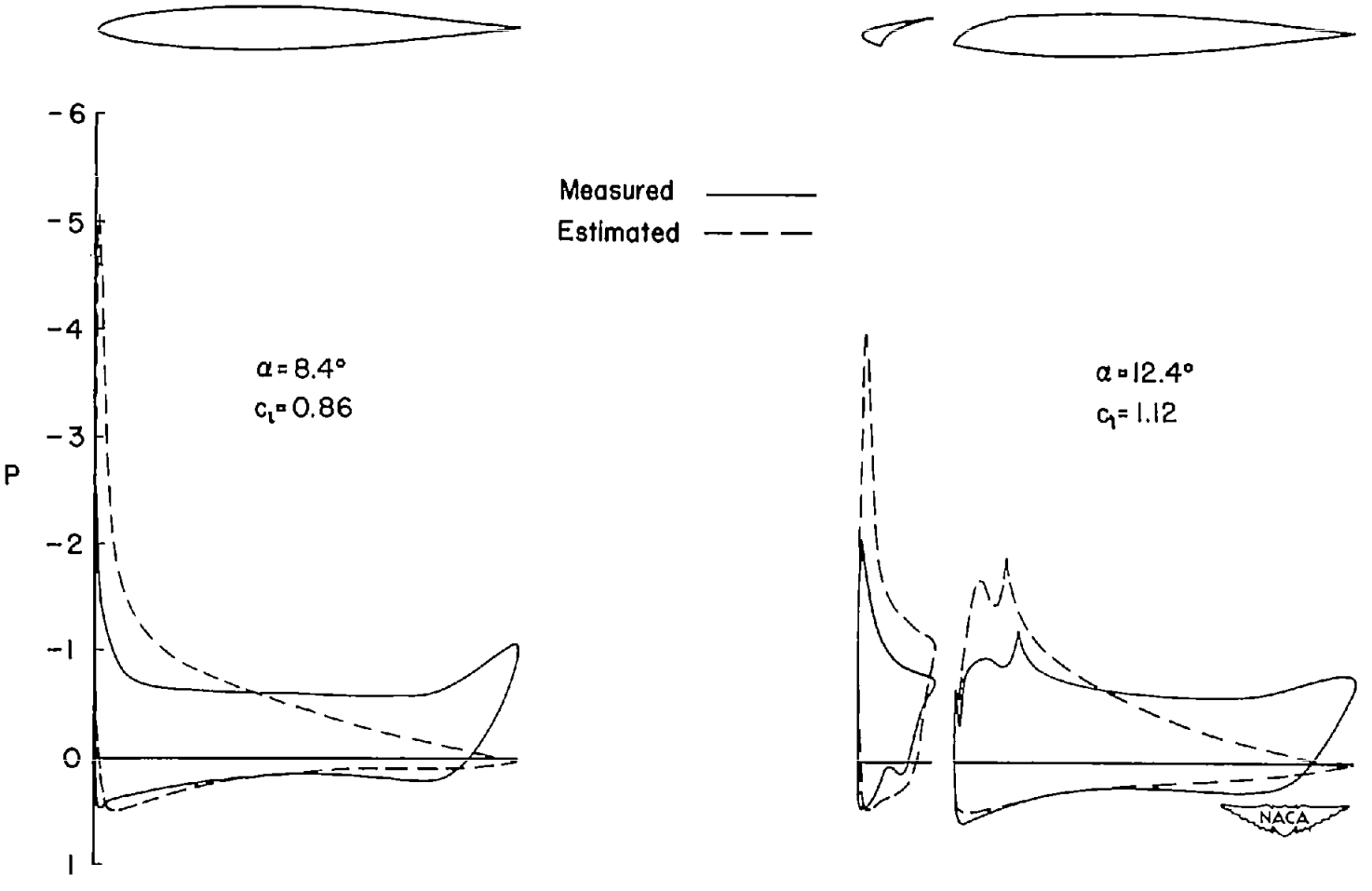

(a) η = 0.17

Figure 7.– Comparisons near maximum lift of measured and estimated pressure distributions at six semispan stations with and without slats. Flaps deflected.

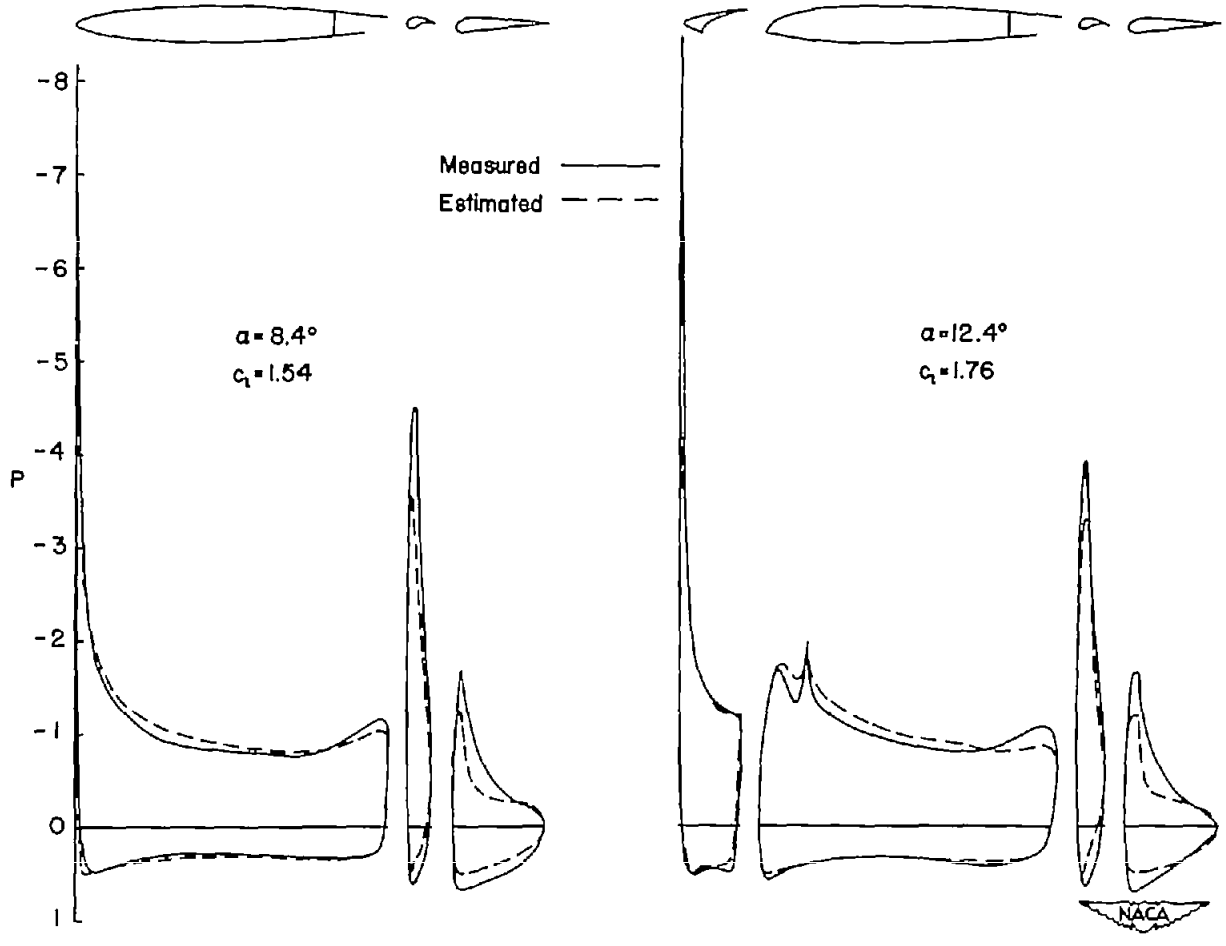

(b) η = 0.38

Figure 7.- Continued.

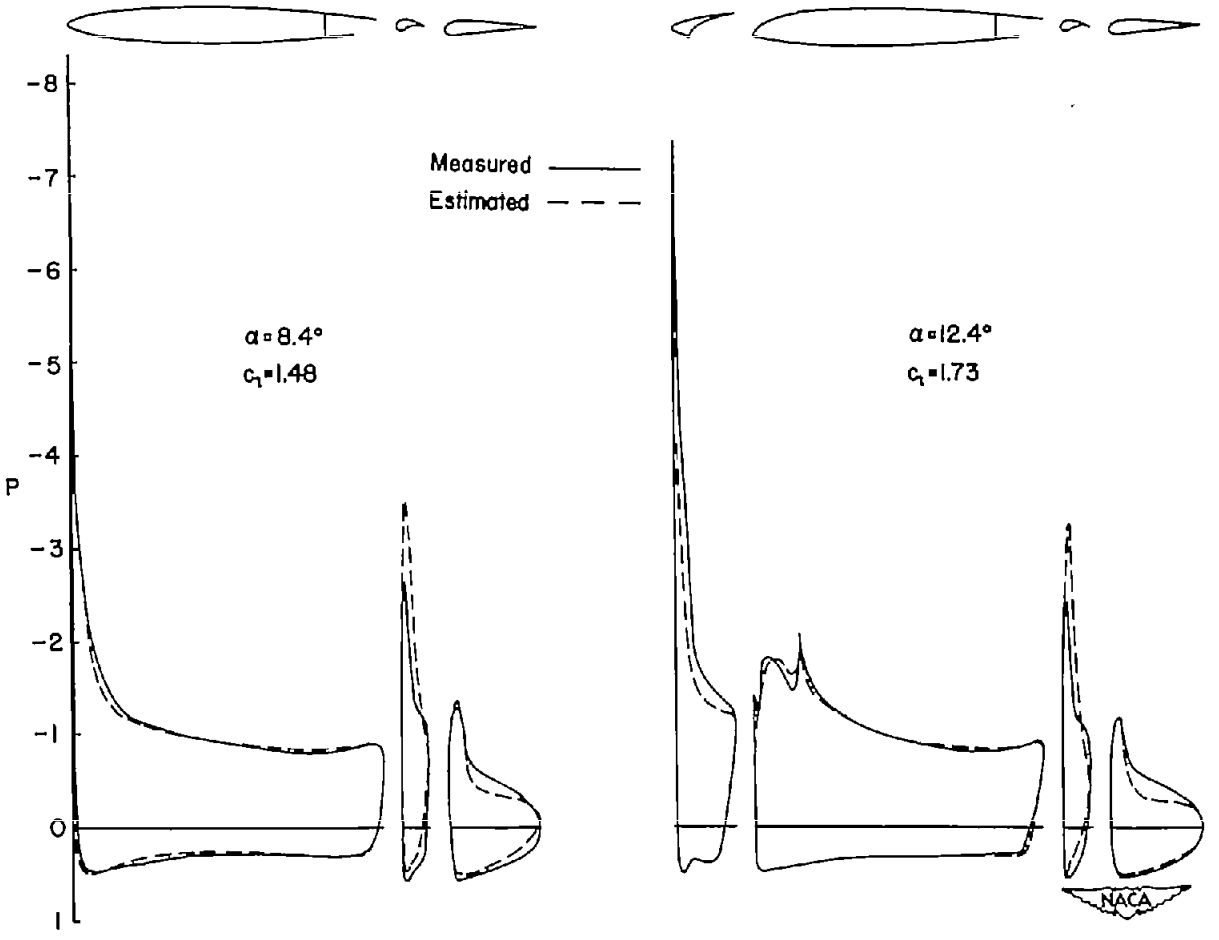

(c) $\eta = 0.55$

Figure 7.– Continued.

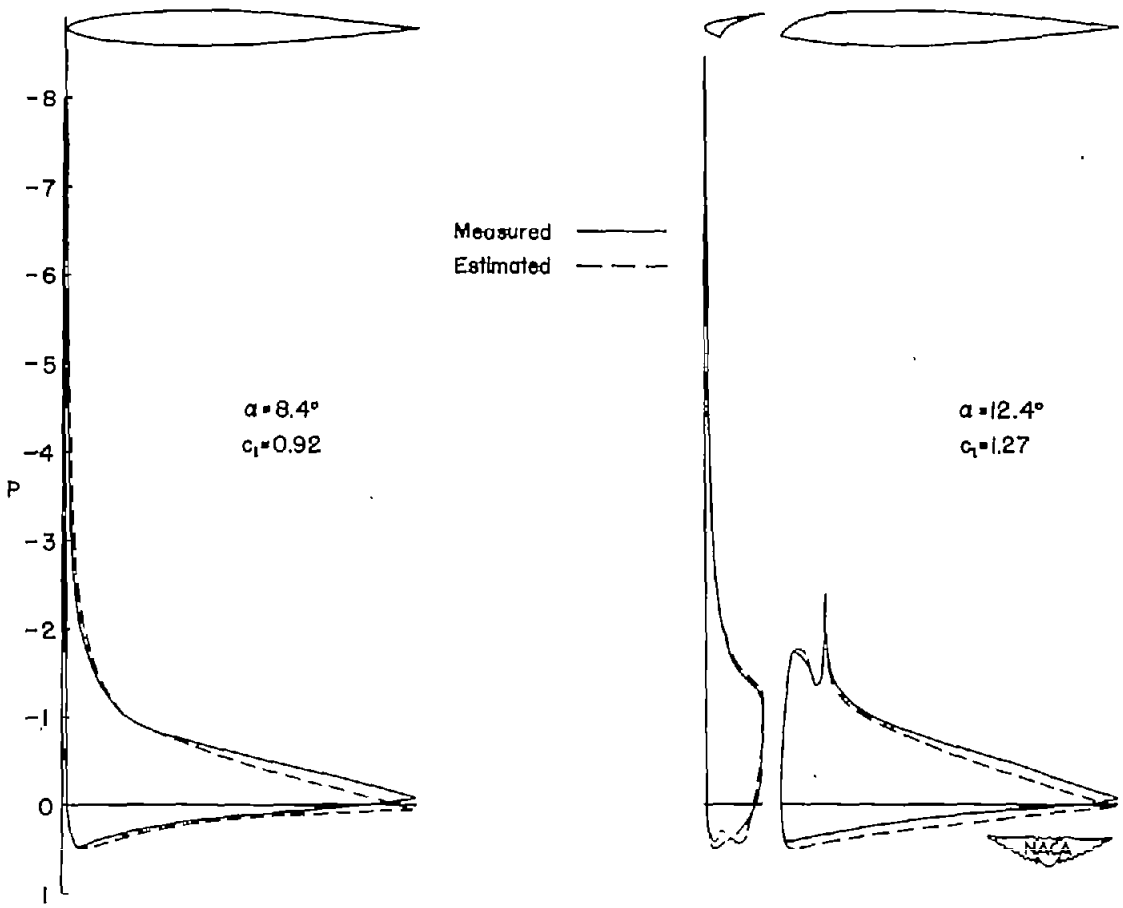

(d) $\eta = 0.71$

Figure 7.– Continued.

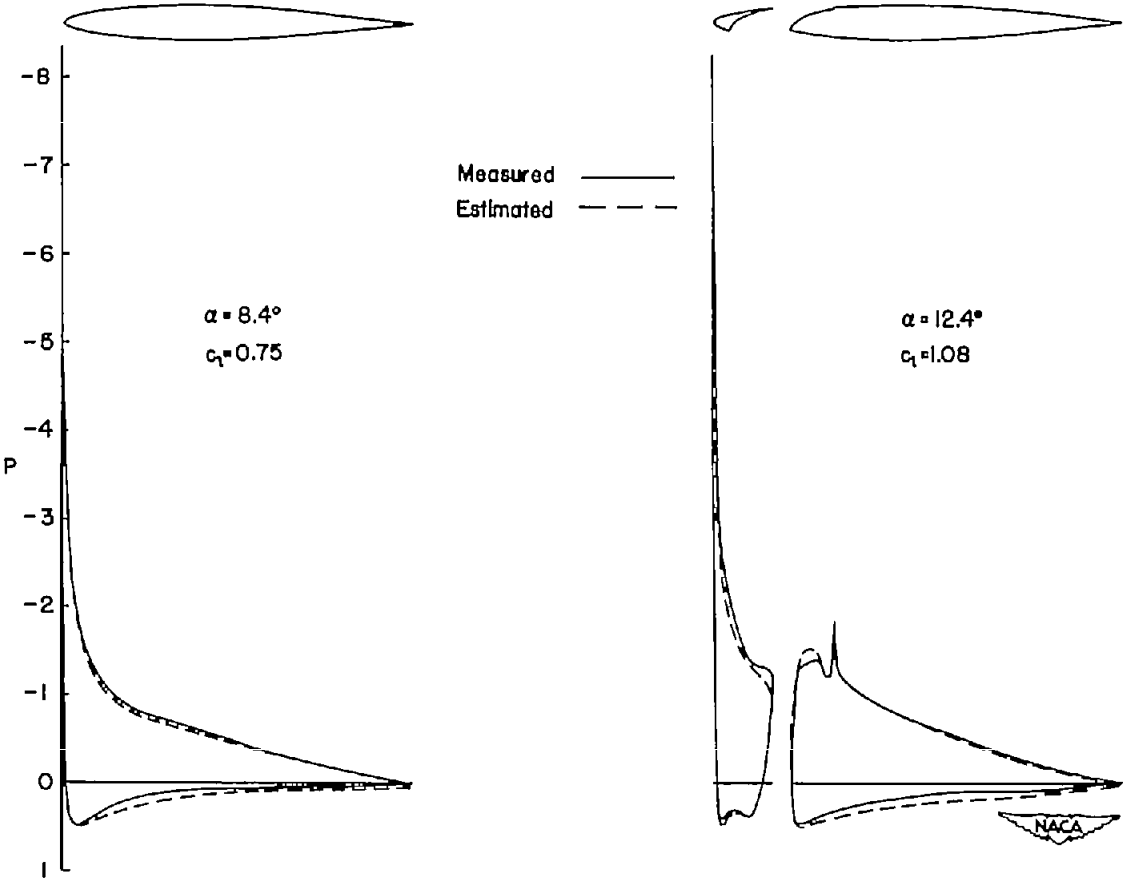

(e) $\eta = 0.82$

Figure 7.– Continued.

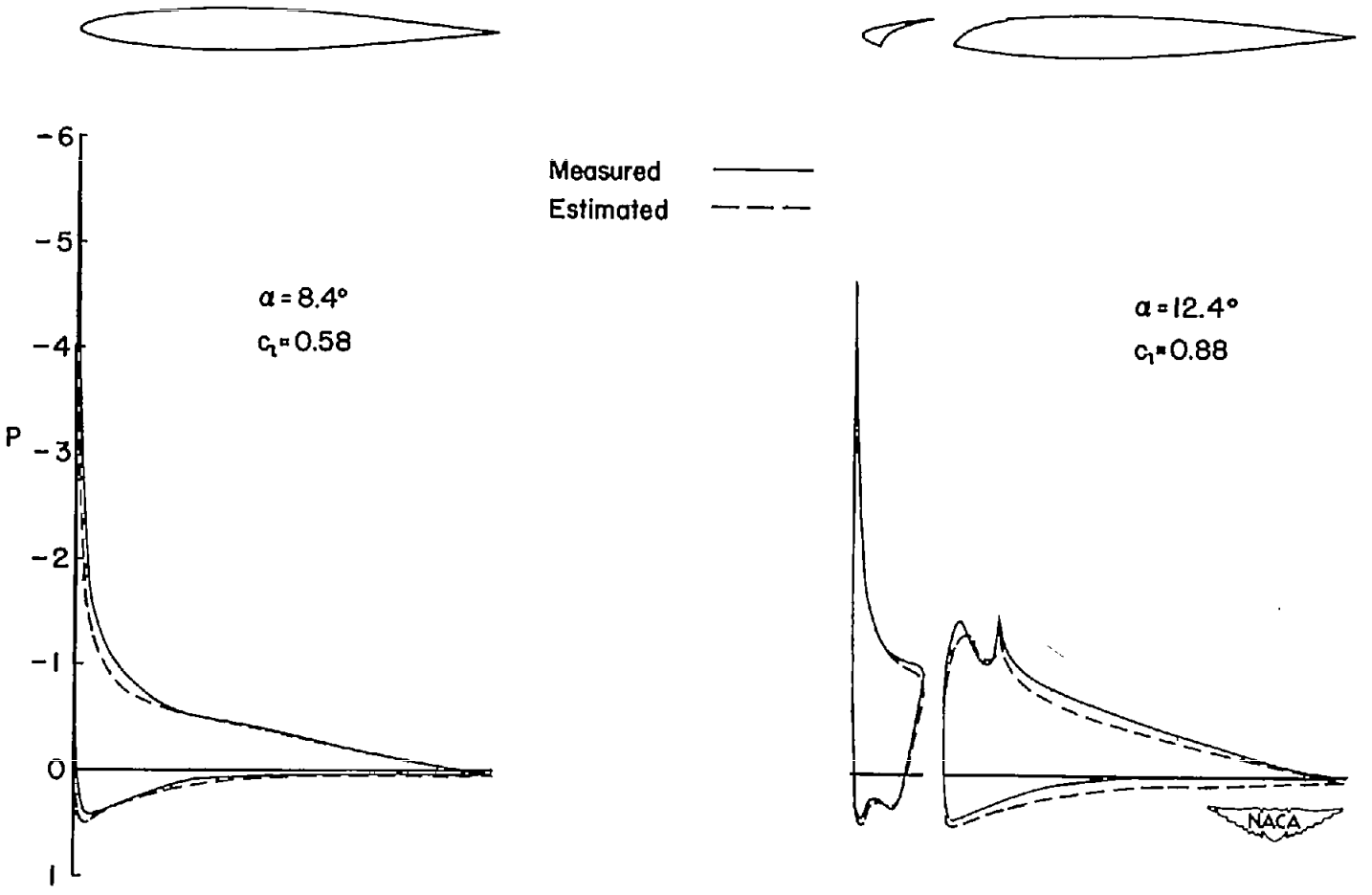

(f) η = 0.92

Figure 7.– Concluded.

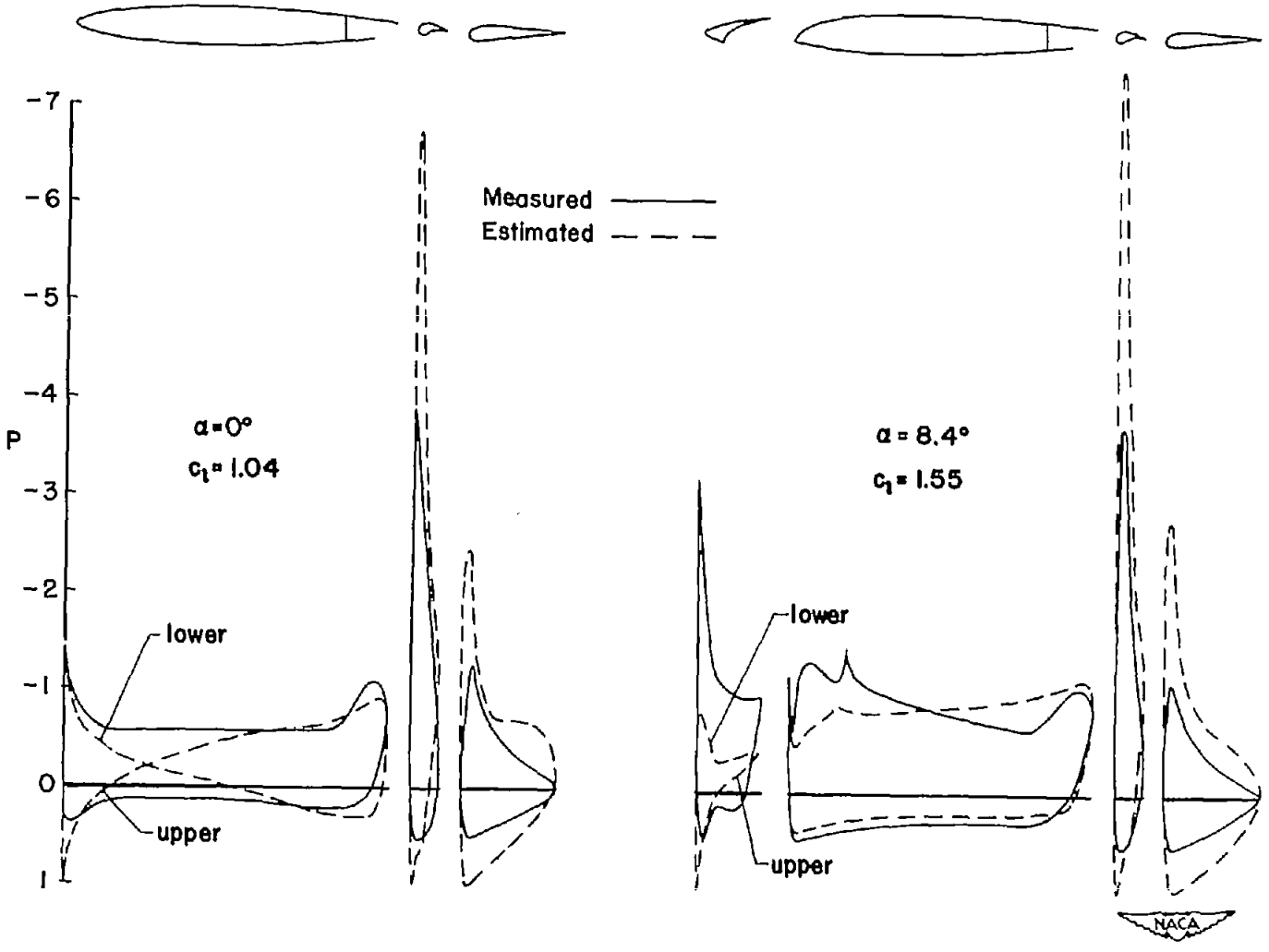

Figure 8.- Examples of pressure-distribution comparisons between measured results for the wing and two-dimensional data uncorrected for sweep. $\eta = 0.55$.

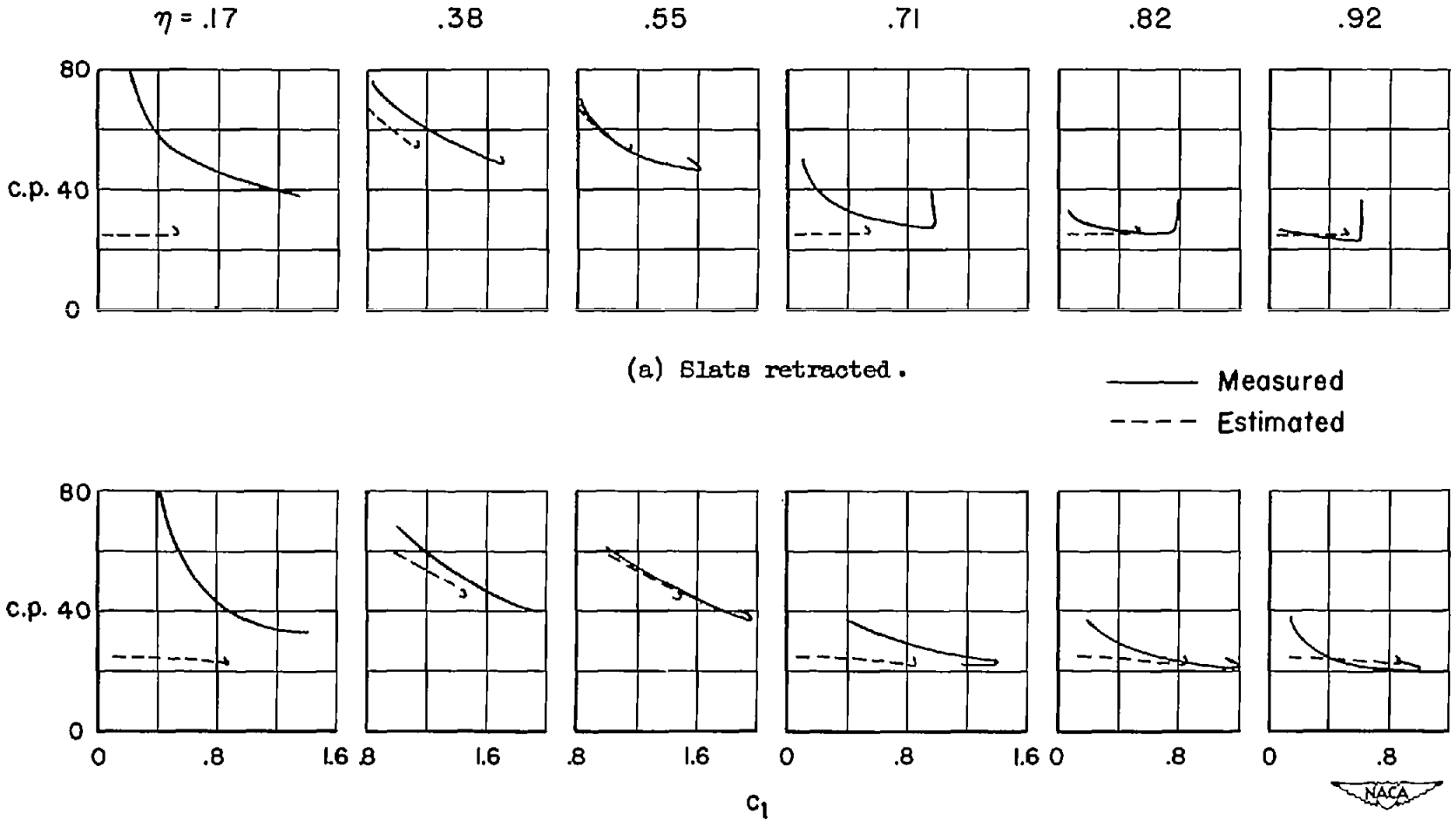

Figure 9.– Comparisons of the measured and estimated variations of local centers of pressure with local lift coefficient.

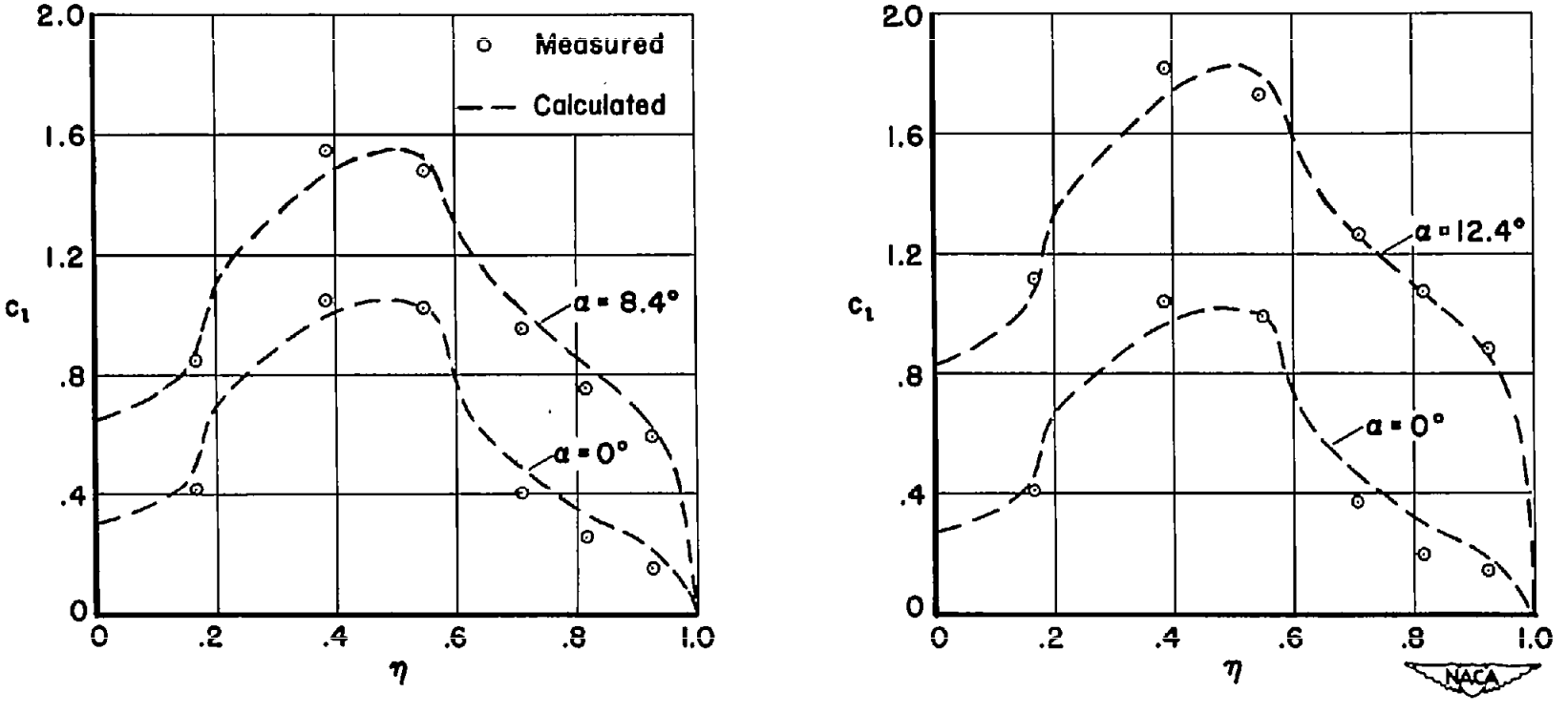

(a) Slats retracted.

(b) Slats extended.

Figure 10.- Comparisons of the measured and calculated spanwise variations of local lift coefficient.

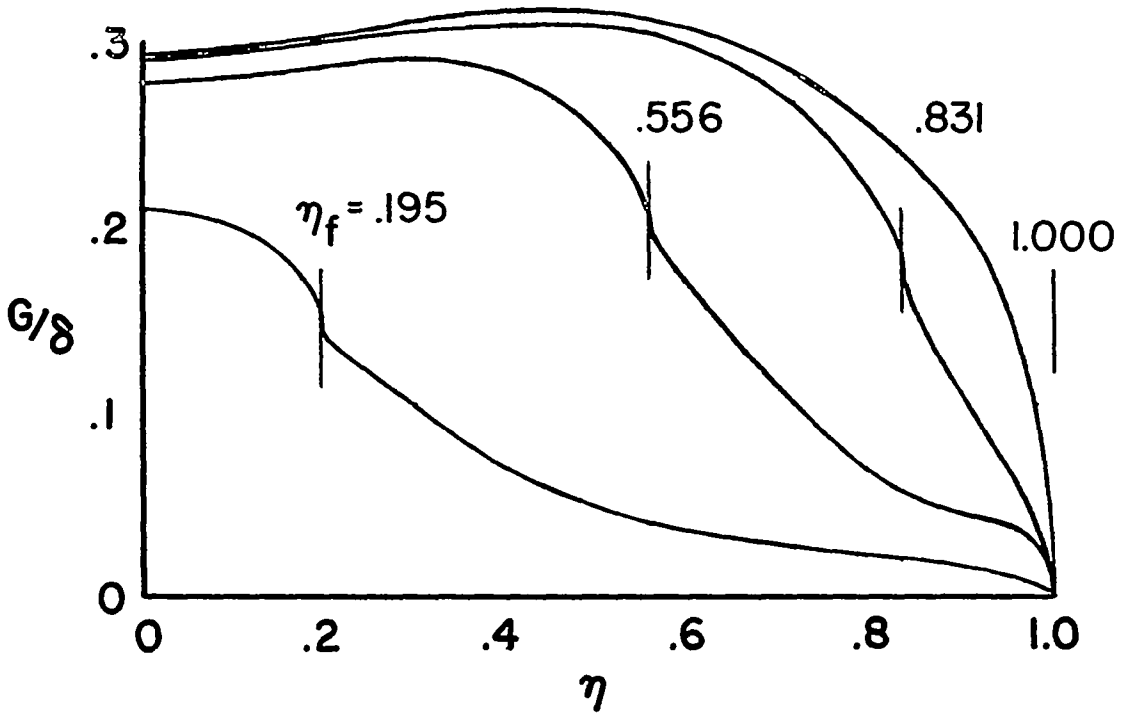

(a) Variation spanwise of the loading coefficient for several flap spans.

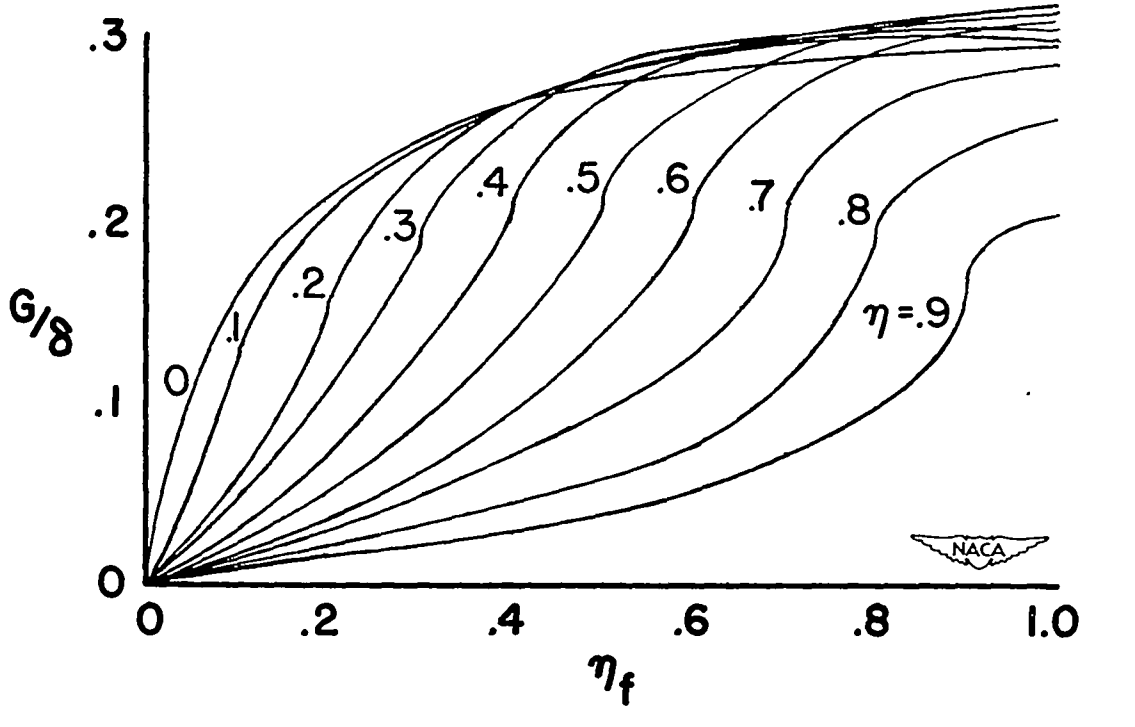

(b) Variation of loading coefficient with flap span.

Figure 11.— Theoretical spanwise load-distribution coefficients due to symmetric flap deflection. c_f/c = 1.0.

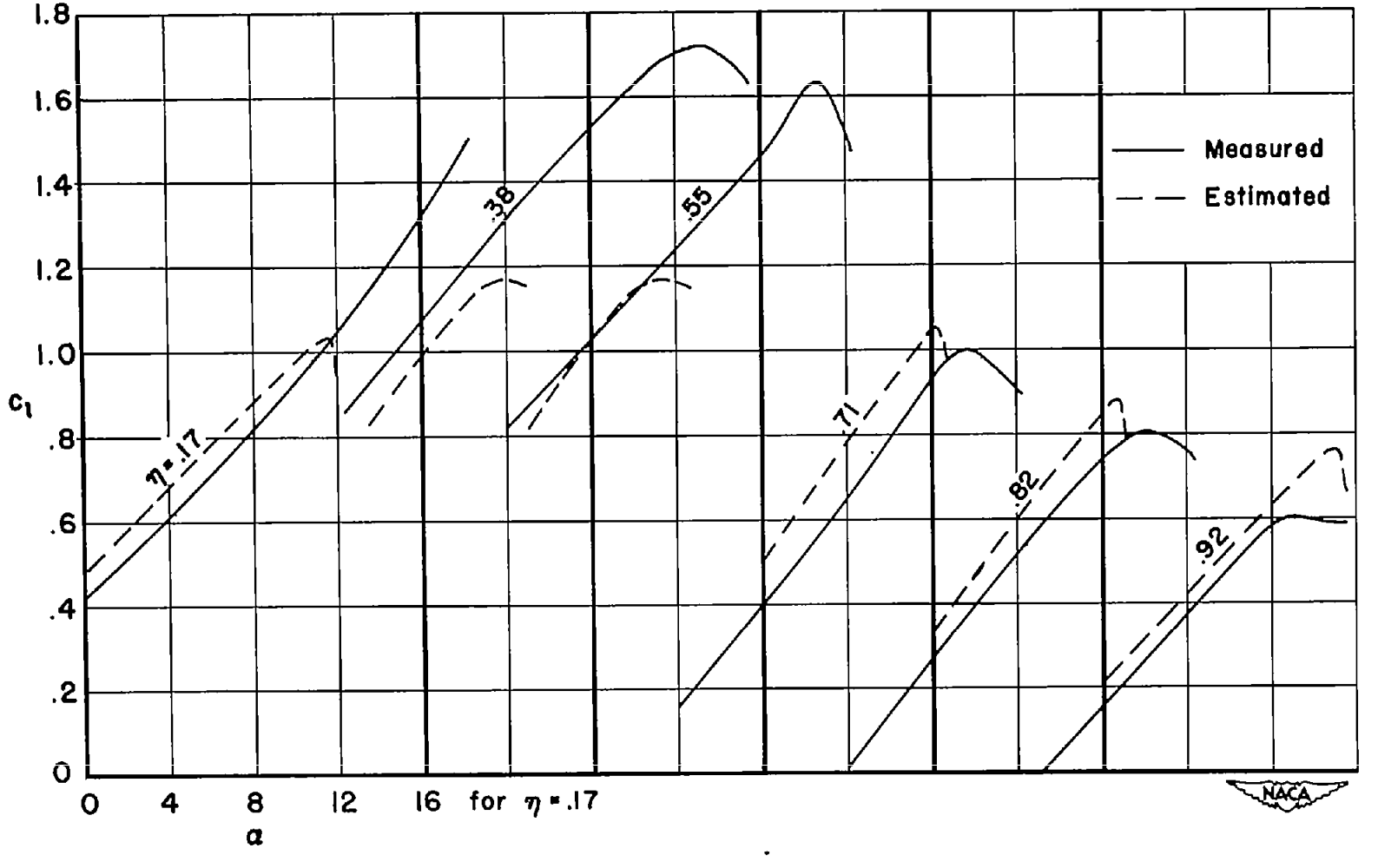

(a) Slats retracted.

Figure 12.– Comparisons of local lift curves measured at six stations on the wing with those estimated from two-dimensional data and span-loading theory.

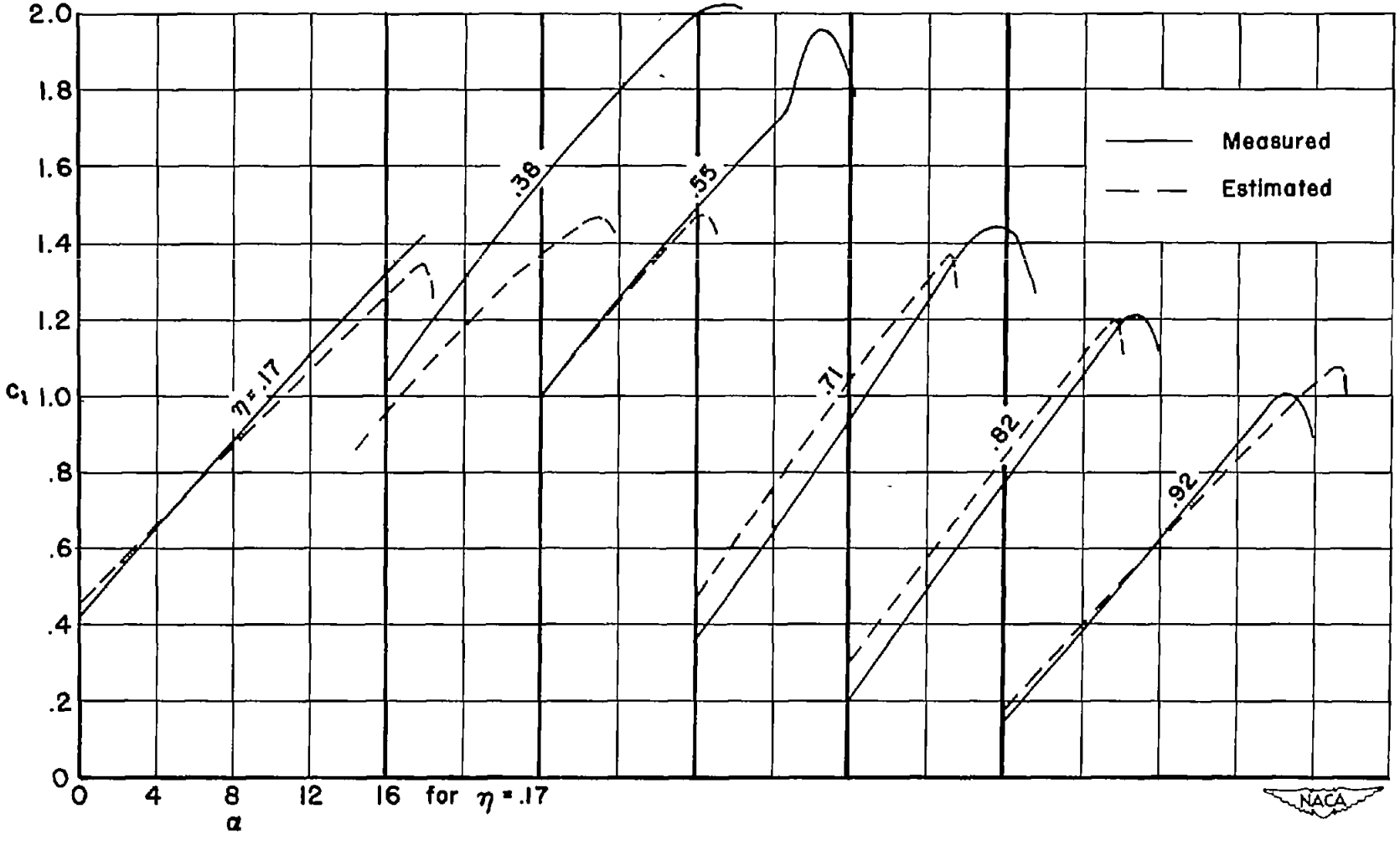

(b) Slats extended.

Figure 12.– Concluded.

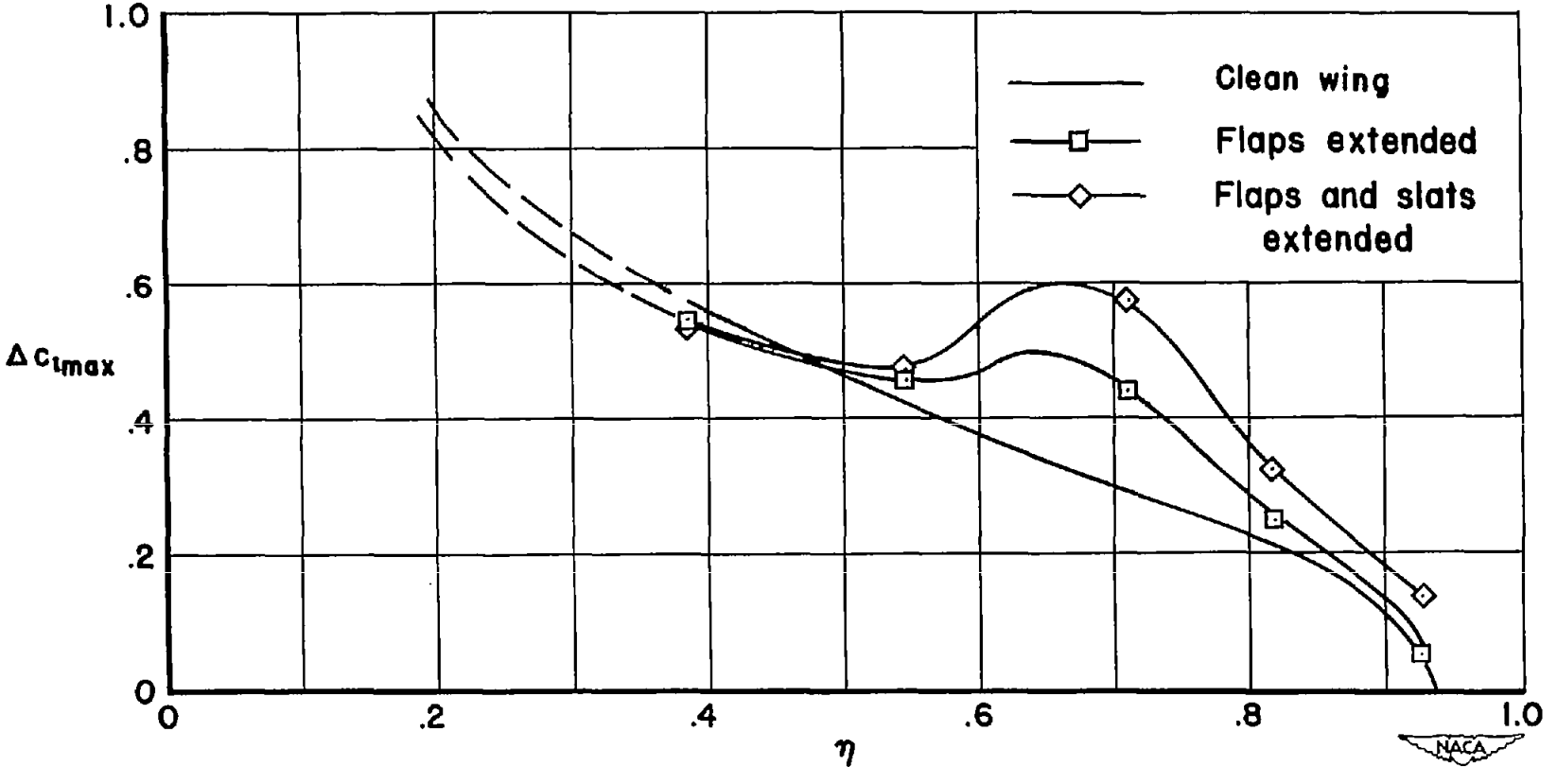

Figure 13.– Variation spanwise of the increment in $c_{l_{max}}$ measured for the swept wing above that for the yawed infinite wing.

NACA-Langley - 11-23-53 - 1000